SMHI RO
No.21, January 1995

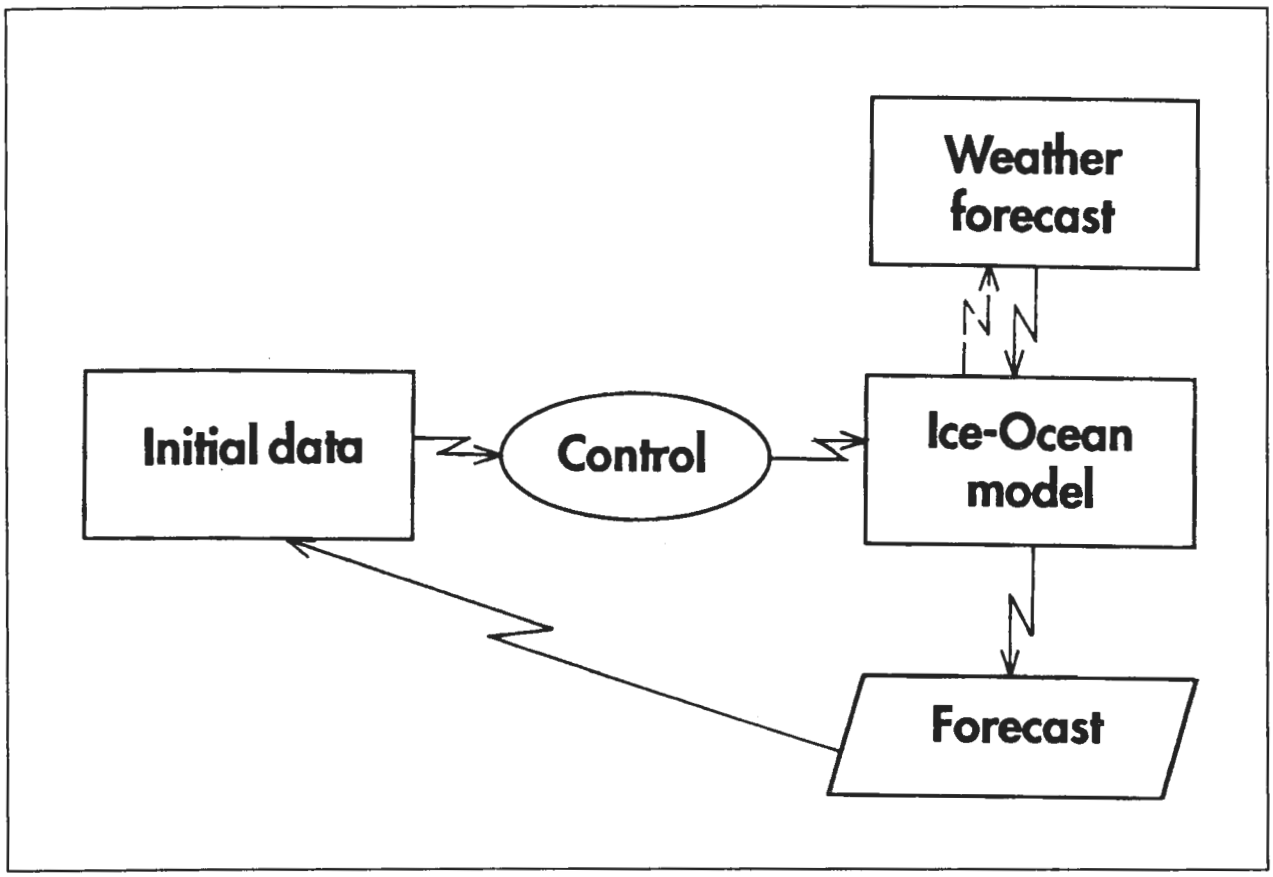

A COUPLED ICE-OCEAN MODEL SUPPORTING WINTER NAVIGATION IN THE BALTIC SEA

Part 2. Thermodynamics and meteorological coupling

Anders Omstedt and Leif Nyberg

SMHI REPORTS OCEANOGRAPHY No.21, January 1995

A COUPLED ICE-OCEAN MODEL SUPPORTING WINTER NAVIGATION IN THE BALTIC SEA

Part 2. Thermodynamics and meteorological coupling

Anders Omstedt and Leif Nyberg

Issuing Agency

SMHI
S-601 76 Norrköping
Sweden

Report number

RO No. 21

Report date

January 1995

Author (s)

Anders Omstedt and Leif Nyberg

Title (and Subtitle)

A coupled ice-ocean model supporting winter navigation in the Baltic Sea
Part 2. Thermodynamics and meteorological coupling

Abstract

For the first time a coupled ice-ocean model system simulating both dynamic and thermodynamic processes has been run operationally for the Baltic Sea. The dynamical part of the system is based upon a two-dimensional coupled ice-ocean model that resolves the horizontal space and time, and the thermodynamic part of the system is based upon a one-dimensional coupled ice-ocean model that resolves the vertical space and time for different regions in the Baltic Sea. The system was forced using meteorological fields from the HIRLAM system and was run in operational mode during the winter of 1993/1994. The forecasted parameters were: water cooling, ice formation, ice growth and decay, ice drift and ridging, vertical mean currents, sea levels and water warming. The general experience from the winter was most satisfactory and the model system forms a good base for forecasts and further research.

During the winter of 1993/1994 a closer coupling between the ice-ocean system and the HIRLAM system has been tested, illustrating the importance of using accurate ice fields in the HIRLAM system.

Key words

Baltic Sea, modelling, forecasting, sea ice dynamics, sea ice thermodynamics, cooling, freezing, ice growth, ice modelling

Supplementary notes

Number of pages

38

Language

English

ISSN and title

0283-1112 SMHI Reports Oceanography

Report available from:

SMHI
S-601 76 NORRKÖPING
Sweden

1. INTRODUCTION

The atmosphere, the ice and the ocean constitute a physical system with strong coupling. Therefore, coupled models are needed for a proper simulation. Within the Swedish-Finnish Winter Navigation Research Program, coupled models are now introduced into operational use. In the winter of 1992/93 a dynamically coupled ice-ocean model for the Baltic Sea (the BOBA model) was applied in operational use at SMHI (Omstedt et al., 1994). The ice model is based upon the Hibler model (1979) and was further developed in Finland by Leppäranta (1981) and Leppäranta and Zhang (1992). The ocean storm surge model was developed in China by Zhang and Wu (1990), and the coupled ice-ocean model applied to the Baltic Sea was first presented by Zhang and Leppäranta (1992). In general the results from the operational use were most promising, but further work was needed, particularly the inclusion of thermodynamics and a closer coupling between the ice-ocean model and the HIRLAM model. Also the development of automatic methods for the generation of initial data to the model was needed.

In the present paper, an extended version of the coupled ice-ocean model (Figure 1) is presented, which includes full thermodynamics (water cooling, ice formation, ice growth/decay and water warming). The thermodynamics were modelled by using similar ideas and models as were developed by Omstedt et al. (1983) and Omstedt (1990 a, b). In the thermodynamic modelling we considered two cases: firstly, an ocean boundary layer forced by the atmosphere, representing the open sea case; secondly, a coupled ice-ocean boundary layer forced by ice drift and energy exchanges, representing the ice case. The thermodynamic model only resolved vertical variations but was applied to different regions in the Baltic Sea. Ideally, one should make thermodynamic calculations in every grid point, but as the number of active points is about 1000, this was not feasible. During the winter of 1993/94 we applied the thermodynamic model to 19 different areas, following the subdivision of the Baltic Sea according to Prof. Jurva (see Seinä and Palosuo, 1993) and Omstedt (1990 a) (Figure 2). Typically, the depth, the vertical resolution, and the meteorological forcing were different for the different regions. For all the cells in a region, the same results of the thermodynamic calculations were applied, but these results, of course, differed from region to region. The model is now named the BOBA-P19 model, as we use the general equation solver PROBE (Svensson, 1986) in 19 subareas for solving the thermodynamic fluxes.

During the winter some tests with a closer coupling between the ice-ocean model and HIRLAM were also performed. The results from these as well as verifications of the HIRLAM forecasts over the Baltic Sea will be presented below.

In Section 2, the model equations related to the new thermodynamic part are given. Then the numerical and operational procedures are outlined. The characteristics of the winter of 1993/94 are given in Section 3, and in Section 4 results from the operational runs are presented. Different aspects of the meteorological forcing and coupling to the ice-ocean model are discussed in Section 5. Finally, a summary with conclusions is given in Section 6.

2. THE MODEL

2.1 The sea ice model

The dynamical parts of the coupled ice-ocean model were discussed in Omstedt et al. (1994), and the reader is referred to this part for further discussion about the dynamics. In the present part we only outline the new model elements that are related to the thermodynamic coupling.

The ice thicknesses and ice concentration are calculated from a three-layer approach. The levels are: open water (1-A_i), level ice thickness (h_l) and ridged ice thickness (h_r). The ice concentration and the ice thicknesses are calculated according to:

$$\frac{\partial}{\partial t}(A_i, h_l, h_r) = -W_i \cdot \nabla(A_i, h_l, h_r) + (\Psi_A, \Psi_l, \Psi_r) + (\Gamma_A, \Gamma_l, \Gamma_r) \tag{1}$$

where W_i is the ice drift, Ψ_A, Ψ_l and Ψ_r are the mechanical deformation functions and Γ_A, Γ_l and Γ_r are the thermodynamic terms. The ice mass is connected to ice concentration, A_i, and ice thickness, h_i, through the following equation of state:

$$m_i = \rho_i h_i A_i = \rho_i (h_l + h_r) A_i \tag{2}$$

The Γ_l term specifies the net ice growth or melt. During freezing Γ_l is given by the sum of the ice growth in open water (frazil ice growth) plus the ice growth over the portion of the cell covered by level ice. During ice-melt Γ_l is given by the melting over the portion of the cell covered by ice. The Γ_l term reads:

$$\rho_i L \Gamma_l = \alpha F_n (1 - A_i) + \left[\frac{k_i k_s}{k_i h_s + k_s h_i} (T_f - T_0) + F_s^{it} - F_s^{ib} - F_w \right] A_i \tag{3}$$

where α is a factor equal to 1 when F_n is positive and 0 when F_n is negative, F_n is the net heat flux at the air/water interface, h_i and h_s are the ice and snow thicknesses, k_i and k_s the thermal conductivity of ice and snow, T_f is the water freezing temperature, T_0 the temperature at the air/snow interface, F_s^{it} and F_s^{ib} the sun radiation at the top and bottom of the ice surface and F_w the heat flux from the sea to the ice. All fluxes are treated as positive in positive vertical space (upwards). The air/snow interface temperature can be obtained by considering the heat energy budget over the snow cover, see Maykut (1986). This is, however, not done in the present model. Instead T_0 is assumed to be equal to the air temperature as long as the temperature is below freezing. The parametrization of the heat fluxes are outlined in Appendix A.

The thermodynamic term associated with ice concentration reads:

$$\Gamma_A = \begin{cases} k_A(A_{\max} - A) & A \le 0.9 \\ 0 & A > 0.9 \end{cases} \qquad (4)$$

where A_{max} is a reference ice concentration equal to 0.9 and k_A a constant equal to $5 \cdot 10^{-5}(s^{-1})$ corresponding to a 50 % increase during a time step of three hours. This is applied in such a way that the total ice mass in a cell is conserved. The thermodynamic growth/decay of ridged ice is assumed to be small, and thus $\Gamma_r = 0$.

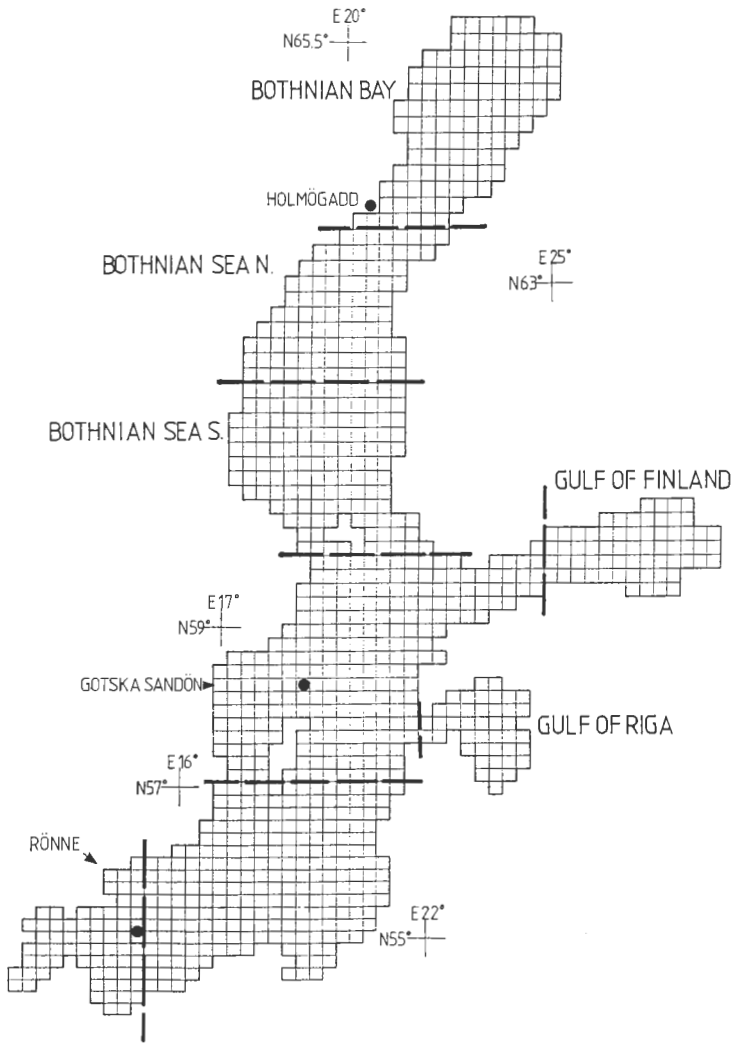

Figure 1.

Grid for the ice-ocean model. In each grid cell sea ice drift and deformation, vertical meancurrents and water levels were calculated. The thick dashed lines indicate how the Baltic Sea was divided into larger regions for the verification study discussed in Section 4.4.

2.2 The ocean models

The effects of the ocean are treated by using two different ocean models. The first treats advection, and the calculations are done by using a two-dimensional storm surge model which is dynamically coupled to the ice model, see Omstedt et al. (1994). The second treats the ice-ocean thermodynamics and calculates the heat exchange by using a one-dimensional turbulent exchange model. In the one-dimensional model, open and ice-covered boundary conditions are included and the model is applied to a number (presently 19) of regions in the Baltic Sea (Figure 2). The ice-ocean thermodynamics as well as the coupling are outlined below.

Figure 2.
Subdivision of the Baltic Sea into 19 thermodynamic regions. In each region water cooling, ice formation, ice growth and decay and water warming were calculated.

Primarily it is the heat fluxes from the ocean to the atmosphere or the ice that are of main interest, but some more variables are needed to describe the upper layers of the ocean. Salinity is one of these, as well as velocity. For basic assumptions etc., see Omstedt et al. (1983) and Omstedt (1990 a). The mean ocean boundary layer equations (neglecting vertical advection) read:

$$\frac{\partial T}{\partial t} = \frac{\partial}{\partial z}\left[\left(\frac{\nu}{Pr_L} + \frac{\nu_T}{Pr_T}\right)\frac{\partial T}{\partial z}\right] + \Gamma_s \tag{5}$$

$$\frac{\partial S}{\partial t} = \frac{\partial}{\partial z}\left[\left(\frac{\nu}{Sc_L} + \frac{\nu_T}{Sc_T}\right)\frac{\partial S}{\partial z}\right] \tag{6}$$

$$\frac{\partial U}{\partial t} = \frac{\partial}{\partial z}\left(\nu_T \frac{\partial U}{\partial z}\right) + fV \tag{7}$$

$$\frac{\partial V}{\partial t} = \frac{\partial}{\partial z}\left(\nu_T \frac{\partial V}{\partial z}\right) - fU \tag{8}$$

$$\rho = \rho_0\left[1 - \alpha_1(T - T_M)^2 + \alpha_2 S\right] \tag{9}$$

where z is the vertical space coordinate positive upwards, t the time coordinate, T the temperature, ρ the density, C_p the specific heat, ν and ν_T are the laminar and turbulent viscosity, Pr_L and Pr_T the laminar and turbulent Prandtl numbers, Γ_s is the source term associated with solar radiation (see Appendix A), S the salinity, Sc_L and Sc_T are the laminar and turbulent Schmidt numbers, U and V the mean currents in horizontal directions, f is the Coriolis parameter, ρ the sea water density, ρ_0 a reference density, T_M the temperature of maximum density, and α_1 and α_2 are constants in the equation of state.

The boundary conditions for an open water surface read:

$$\left(\frac{\nu}{Pr_L} + \frac{\nu_T}{Pr_T}\right)\frac{\partial T}{\partial z} = F_n(\rho_0 C_p)^{-1} \tag{10}$$

$$\left(\frac{\nu}{Sc_L} + \frac{\nu_T}{Sc_T}\right)\frac{\partial S}{\partial z} = 0 \tag{11}$$

$$\nu_T \frac{\partial U}{\partial z} = -\tau_x^a \rho_0^{-1} \tag{12}$$

$$\nu_T \frac{\partial V}{\partial z} = -\tau_y^a \rho_0^{-1} \tag{13}$$

where τ_x^a and τ_y^a are the wind stresses in the x- and y-directions. A zero flux condition is assumed for the salinity equation, even though precipitation and evaporation may produce a net flux. The wind stress was calculated using a standard bulk formulation:

$$\begin{aligned} \tau_x^a &= \rho^a C_a^i U^a |W^a| \\ \tau_y^a &= \rho^a C_a^i V^a |W^a| \end{aligned} \tag{14}$$

where $|W^a|$ is the wind speed, U^a and V^a are the wind velocity components in the x- and y-directions and C_a^i is an air drag coefficient.

In the case of ice, the boundary conditions for temperature are:

$$\begin{aligned} T = T_f &= -0.0575 \cdot S_0 + 1.710523 \cdot 10^{-3} S_0^{3/2} - 2.154996 \cdot 10^{-4} S_0^2 \\ \left(\frac{\nu}{Pr_L} + \frac{\nu_T}{Pr_T}\right)\frac{\partial T}{\partial z} &= F_w (\rho_0 C_p)^{-1} \end{aligned} \tag{15}$$

where S_0 is the interfacial salinity and F_w the heat flux between water and ice. The boundary condition for salinity at the ice/water interface is assumed to be related to the freezing and melting rate:

$$\left(\frac{\nu}{Sc_L} + \frac{\nu_T}{Sc_T}\right)\frac{\partial S}{\partial z} = \frac{\rho_i}{\rho_0}\frac{dh_i}{dt}(S_0 - S_i) \tag{16}$$

where S_i is the ice salinity. The corresponding boundary conditions for momentum is:

$$\nu_T \frac{\partial U}{\partial z} = -\tau_x^i \rho_0^{-1} \tag{17}$$

$$\nu_T \frac{\partial V}{\partial z} = -\tau_y^i \rho_0^{-1} \tag{18}$$

where τ_x^i and τ_y^i are the ice-water stresses in the x- and y-directions, which was calculated from:

$$\begin{aligned} \tau_x^i &= \rho_0 C_w^i (U_i - U)|W_i - W_c| \\ \tau_y^i &= \rho_0 C_w^i (V_i - V)|W_i - W_c| \end{aligned} \tag{19}$$

were W_i is the ice drift, W_c the current and C_w^i an ice water drag coefficient. The conditions for the lower boundary are no flux conditions, except for velocity, for which a zero velocity condition is used.

To bridge the fully turbulent ocean layer beneath the drifting ice and the viscous sublayer adjacent to the ice, two model approaches are available today. The first one introduces wall functions (Mellor et al., 1986) and puts the near-wall mesh point into the fully turbulent fluid. The second one introduces a low-Reynolds' number turbulence model for the viscous region (Svensson and Omstedt, 1990) and resolves the whole boundary layer all the way into the ice. In the present model we apply wall functions.

McPhee et al. (1987) tested different wall function formulations and illustrated that fully turbulent models predicted unrealistically high melting rates and that the viscous sublayer models underestimated melting. Quite realistic values were, however, received using a wall function formulation according to Yaglom and Kader (1974). In the present paper we shall follow that path, and the wall functions read:

$$St_T^{-1} = b \left(\frac{u_* z_0}{\nu} \right)^{0.5} Pr_L^{0.67} \tag{20}$$

$$St_S^{-1} = b \left(\frac{u_* z_0}{\nu} \right)^{0.5} Sc_L^{0.67} \tag{21}$$

where St_T and St_S are the Stanton numbers for temperature and salinity, respectively, b (= 1.57) is a constant, u_* the friction velocity, z_0 the ice/water roughness parameter, Pr_L (= 13.8) the laminar Prandtl number and Sc_L (= 2432) the laminar Schmidt number. The constants follow McPhee et al. (1987). The roughness height, z_0, is assumed to be constant and equal to 0.05 m according to Leppäranta and Omstedt (1990).

The net heat flux (F_n) to the air/water interface reads:

$$F_n = F_h + F_e + F_{lu} - F_{ld} + F_i \tag{22}$$

where F_h is the sensible heat flux, F_e the latent heat flux, F_{lu} the long-wave radiation upwards, F_{ld} the long-wave radiation downwards and F_i the heat flux associated with ice advection into the grid cell. The parametrization of the heat fluxes can be found in Appendix A.

The turbulence model used is a buoyancy-extended two-equation model of turbulence; one equation for the turbulent kinetic energy, k, and another for the dissipation rate of turbulent kinetic energy, ϵ. The generation of turbulence is calculated from current shear, associated with the wind or the ice drift, and buoyancy production, associated with cooling to the temperature of maximum density and salt rejection due to freezing ice.

The turbulence equations read:

$$\frac{\partial k}{\partial t} = \frac{\partial}{\partial z}\left(\frac{\nu_T}{\sigma_k}\frac{\partial k}{\partial z}\right) + P_s + P_b - \epsilon \tag{23}$$

$$\frac{\partial \epsilon}{\partial t} = \frac{\partial}{\partial z}\left(\frac{\nu_T}{\sigma_\epsilon}\frac{\partial \epsilon}{\partial z}\right) + \frac{\epsilon}{k}\left(C_{1_\epsilon}P_s + C_{3_\epsilon}P_b - C_{2_\epsilon}\right) \tag{24}$$

$$P_s = \nu_T\left[\left(\frac{\partial U}{\partial z}\right)^2 + \left(\frac{\partial V}{\partial z}\right)^2\right] \tag{25}$$

$$P_b = \nu_T\, g\left[-\frac{2\alpha\left(T - T_M\right)}{\sigma_H}\frac{\partial T}{\partial z} + \frac{\beta}{\sigma_s}\frac{\partial S}{\partial z}\right] \tag{26}$$

$$\nu_T = C_\mu\frac{k^2}{\epsilon} \tag{27}$$

where P_s is the production due to shear, P_b production/destruction due to buoyancy, σ_k and σ_ϵ are Prandtl/Schmidt numbers, C_μ, $C_{1\epsilon}$, $C_{2\epsilon}$ and $C_{3\epsilon}$ constants, see Table 1. The surface boundary conditions for turbulent kinetic energy, k, and its dissipation rate, ϵ, are related to the friction velocity and the buoyancy flux at the air/sea interface. At the lower boundary, a zero flux condition is used.

Table 1. The parameters and constants in the coupled ice-ocean model.

Parameters and constants		Value	Unit
ρ_a	Density of air	1.3	kg m^{-3}
ρ_i	Density of ice	910	kg m^{-3}
ρ_w	Reference density of water	10^3	kg m^{-3}
C_{ai}	Drag coefficient of air	1.8×10^{-3}	-
θ_a	Boundary layer angle in air	0	°
C_{wi}	Drag coefficient of water	3.5×10^{-3}	-
θ_w	Boundary layer angle in water	20	°
P^*	Strength constant of ice	10^4	Nm^{-2}
C	Reduction constant for opening	20	-
h_{cr}	Maximum thickness of rafting	0.1	m
h_s	snow thickness	0.1	m
k_i	thermal conductivity of ice	2.0	$Wm^{-1} K^{-1}$
k_s	thermal conductivity of snow	0.3	$Wm^{-1} K^{-1}$
L_i	latent heat of ice	$3.34 \cdot 10^5$	$J kg^{-1}$
α_1	constant in the equation of state	$5.6 \cdot 10^{-6}$	$(°C)^{-2}$
α_2	constant in the equation of state	$8.1 \cdot 10^{-4}$	$(‰)^{-1}$
C_p	specific heat of water	$4.2 \cdot 10^3$	$J kg^{-1} K^{-1}$
C_μ	constant in the turbulence model	0.09	-
$C_{1\epsilon}$	constant in the turbulence model	1.44	-
$C_{2\epsilon}$	constant in the turbulence model	1.92	-
$C_{3\epsilon}$	constant in the turbulence model	0.8	-
σ_k	Prandtl/Schmidt number	1.4	-
σ_ϵ	Prandtl/Schmidt number	1.3	-

2.3 Numerical procedure

The numerical calculations were made in a horizontal grid with a constant grid size of 10 nautical miles (Figure 1). The numerical approach for the dynamical parts of the system was outlined in Omstedt et al. (1994) and the different sub-models are summarized in Table 2.

Table 2. Model elements in BOBA-P19. The elements indicated by (x, y, t) are solved in horizontal space and time. The elements indicated by ($\bar{x}$, $\bar{y}$, z, t) are solved in vertical space and time for different regions.

Elements		Model	Main references
W_i (x, y, t)	ice drift	BOBA	Hibler (1979), Leppäranta
A_i, (x, y, t)	ice concentrations	"	(1981), Leppäranta and
h_l (x, y, t)	level ice thickness	"	Zhang (1992).
h_r (x, y, t)	ice ridging	"	
W_c (x, y, t)	vertical mean current	"	Zhang and Wu (1990), Zhang
η (x, y, t)	water level	"	and Leppäranta (1992).
h_l ($\bar{x}$, $\bar{y}$, t)	level ice thickness	PROBE	
A_i ($\bar{x}$, $\bar{y}$, t)	ice concentration	"	Svensson (1979), Omstedt et
T_w ($\bar{x}$, $\bar{y}$, z, t)	water temperature	"	al. (1983), Omstedt (1990 a).
S_w ($\bar{x}$, $\bar{y}$, z, t)	salinity	"	

The thermodynamic processes were modelled in 19 different regions, as sketched in Figure 2. Each region was represented by the mean depth and the position. Water temperatures were calculated by applying a vertically resolved ocean boundary model to each of these areas. When the temperatures were below the freezing point, the ice boundary conditions were applied, and the changes in ice thickness and ice concentration were calculated. No horizontal coupling between the 19 subareas was assumed. The ocean boundary layer equations were solved by using the general equation solver PROBE (Svensson, 1986), with a time step of 600 s and a vertical resolution depending upon depths of up to 23 grid cells.

2.4 Operational procedure

The BOBA-P19 model system was initialized on the 5 November, 1993, using the ocean fields from the PROBE-BALTIC model (Omstedt, 1990 c) and observed sea surface temperatures. On the basis of the HIRLAM system, weather forecasts including pressure, wind, air temperature, humidity and total cloudiness, for every third hour up to 48 hours were extracted and used as forcing fields for the ice-ocean system. Each day during the winter until 27 May, 1994, 48 hours' forecasts were made. The ice-ocean fields were automatically updated on the basis of the 24 hours' forecasts (Figure 3). During these nearly 7 months, the initial fields were manually corrected on an average of one minor correction each week. Typical corrections were: changes in the mean sea level compensating for in- and outflows to the Baltic Sea, small temperature corrections in the upper sea surface layer and modifications in the ice concentration fields when new satellite information was available. Fast ice was not active in the calculations, instead cells with fast ice were treated as land.

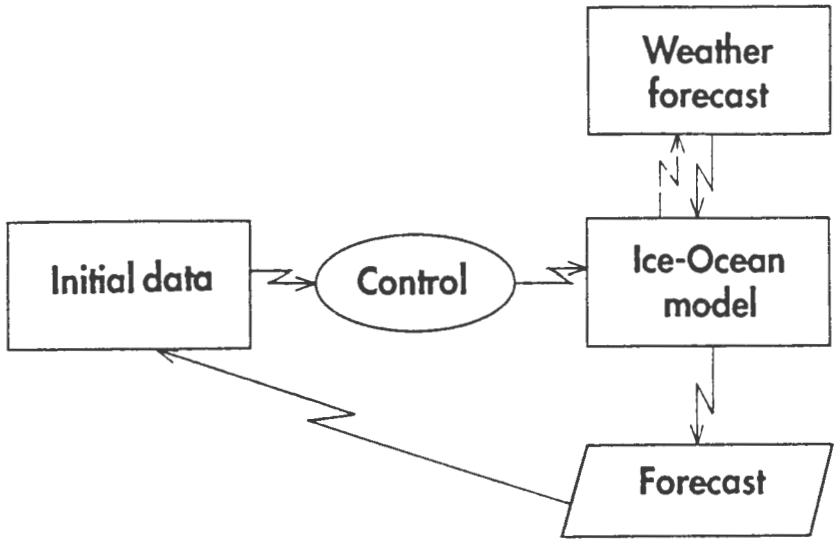

Figure 3.
Schematic presentation of the operational model structure

The time step in the main program of the ice drift model is 3 hours. After initialization and reading of the first weather data set, the storm surge routine is called, and water levels and currents are calculated during 3 steps of one hour each. After completion of this, the 19 PROBE models are called, one by one, and run for 18 time steps of 10 minutes (= 3 hours). The same weather data are, of course, used as forcing during all 18 time steps, but new termodynamics fluxes are calculated every 6th step, in order to account for the sun´s position above the horizon in a reasonable way. The results passed from the PROBE models are formulated as ice increments, as run of ice produced or melted per 3 hours and per unit area. After this, the main ice drift program is run, and ice drift and ice ridging etc. calculated. Then, the ice increments from the PROBE are applied, for each of the 989 active grid points individually, but with the same value for every cell within each of the 19 presented regions. Finally, mean values of ice concentration and thickness for each region are calculated, to be used as starting input to the PROBEs for the next timestep.

After reading of a new weather data set, the above procedure is then repeated up to 16 times (=48 hours). The coupled ice-ocean system was run on a VAX 6000/610 computer, and for a 48 hours forecast about 1 minute CPU-time was required.

3. THE WINTER OF 1993/94

During the winter of 1993/94, the sea ice conditions in the Baltic Sea were normal after six mild winters. The ice formation started in mid and late November, 1993, in the Gulf of Finland and in the northern parts of the Bothnian Bay, respectively. In the middle of December the temperatures decreased and ice started to form in the Bothnian Bay. Due to winds, ice ridges were formed during December and January. In February a high pressure system dominated the weather in the northern parts of the Baltic Sea, giving more ice. Later on leads and ridged ice were forming due to variable winds. The maximum ice extent was reached on March 3. At that time ice was found down to the northern Baltic Proper, in the Gulfs of Finland and Riga. Ice was also formed in the archipelagos and thin ice was observed in the Kattegat. Strong winds in March formed ridged ice fields, and in late March the ice melting started. Due to warm weather in April the ice melted rapidly and disappeared at the end of May.

4. ILLUSTRATIONS

4.1 Ice formation

To illustrate the model, and particularly the thermodynamic part, we first present one example from early winter of calculated ice concentrations and thicknesses. In the end of December, the Bothnian Bay was rapidly covered by ice and almost completely ice-covered on December 28. Due to strong winds, the ice broke up and the ice cover was reduced two days later. In Figure 4, the 48 hour forecast from December 28 is illustrated. The 24 hours forecast showed only small changes in the ice mass, but the 48 hours forecast predicted considerable reduction of ice in the Bothnian Bay (Figure 4, a and b). The reason was higher winds that mixed warmer water from deeper parts up into the surface layer. When comparing the forecast with ice charts from the same period (Figure 5) as well as comparing the calculated (Figure 4 c) and observed ice thicknesses we can see a good agreement.

The example illustrates the importance of considering the heat exchange from water to ice, particularly in early winter.

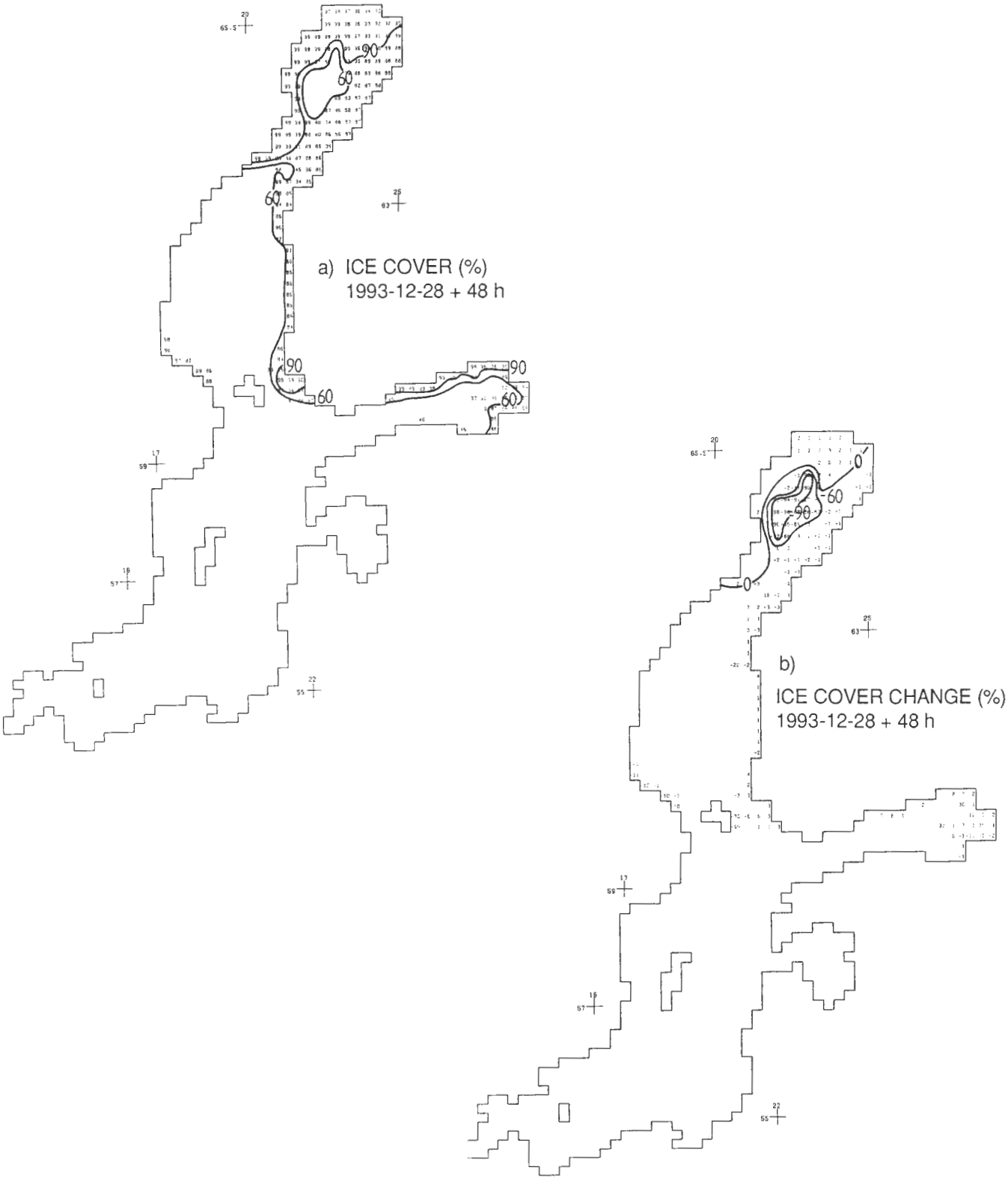

Figure 4.
A 48 hours´ Forecast from December 28, 1993, of ice concentrations (a), changes during the last 24 hours of ice concentrations (b), and ice thicknesses (c).

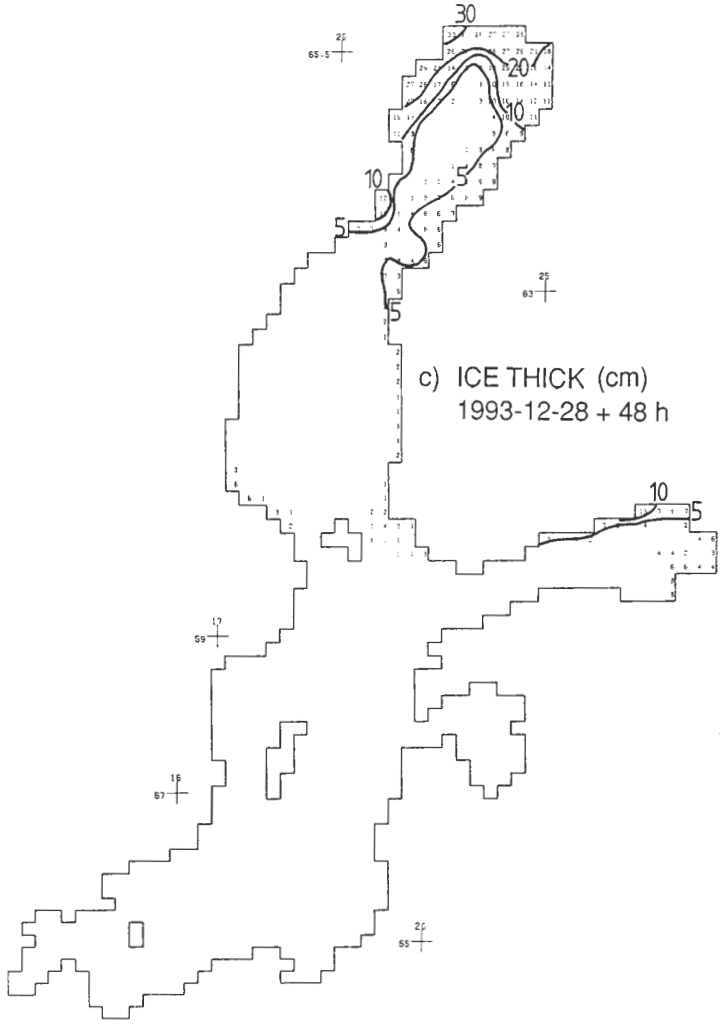

Figure 4 c.

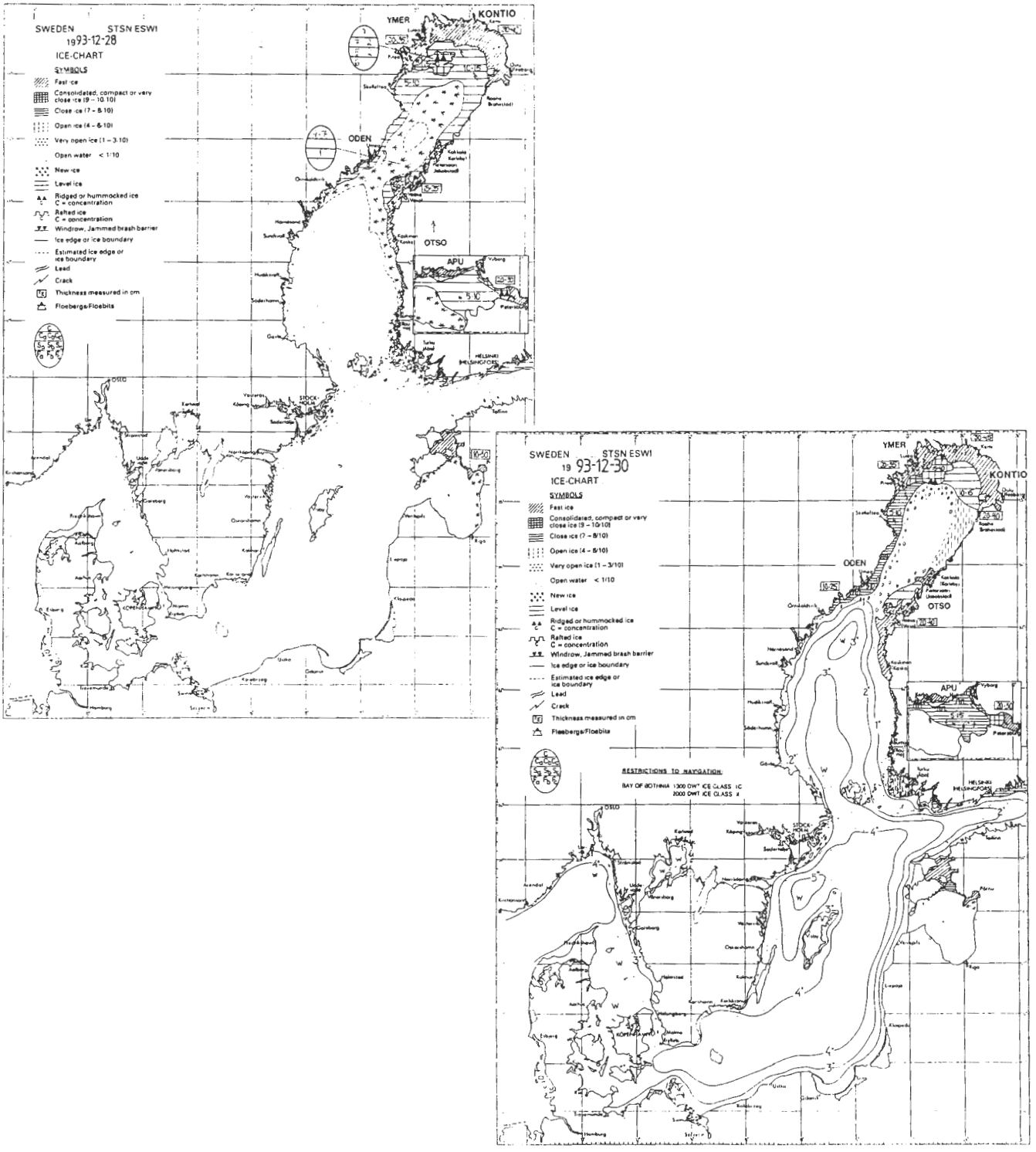

Figure 5. Observed ice conditions on December 28 (a) and 30 (b), 1993

4.2 Maximum ice extent

The maximum ice extent during the winter of 1993/94 was reached on March 3 (Figure 6).

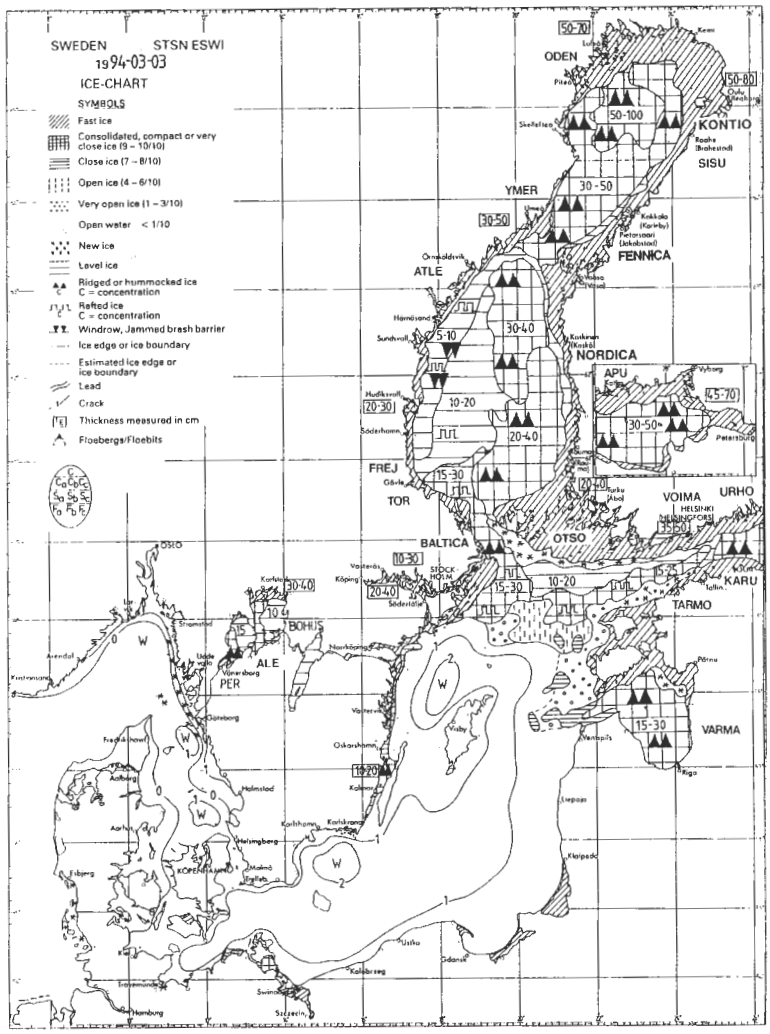

Figure 6.
Observed ice conditions at maximum ice extent during the winter of 1993/1994.

The corresponding model simulations are illustrated in Figure 7 on the basis of a 48 hours forecast issued on March 1. The ice concentrations (Figure 7 a) show that the ice extent is well captured by the model. Notice also that the model indicates ice even in the entrance area of the Baltic Sea. The changes in ice concentrations (Figure 7 b) show an increase along the western coast and a decrease along the eastern coast. These changes were associated with the ice drift (Figure 7 d) moving the ice westward, illustrating that the maximum ice extent was partly due to thermodynamic processes and partly due to dynamic processes. The ice from, for example, the Gulf of Riga was thus advected towards the Baltic Proper and expanding the ice extent in the beginning of March. The ice thicknesses

are illustrated in Figure 7 c. The thin ice is less thick in the model compared to the observations, but the forecast is in general in good agreement with the observations. Also from the ice thicknesses (Figure 7 c) the different thermal regions can be noticed; as we only treat the thermodynamic coupling in 19 regions, the ice thicknesses in these regions become rather homogeneous. By increasing the number of regions, a better resolution can be achieved, but probably only a few more regions need to be incorporated. As the coupled ice-ocean model has now 989 wet grid cells, it is a great advantage that we only need to consider the thermodynamic coupling in about 20 regions.

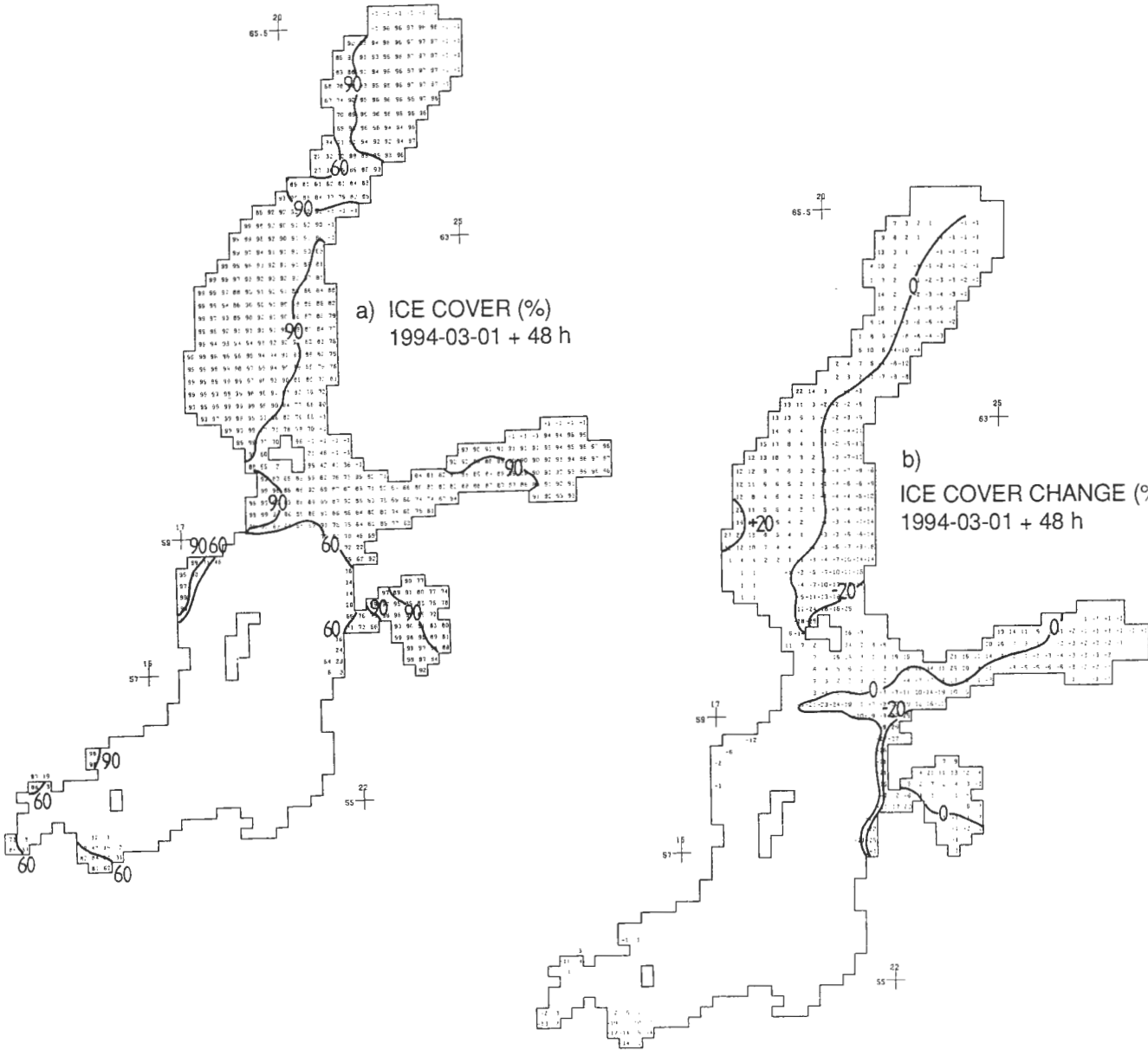

Figure 7.
Calculated ice concentrations (a), changes in ice concentrations during the last 24 hours (b), ice thicknesses (c) and ice drift (d) on March 3, 1994, based upon a 48 hours` forecast. Fast ice is denoted by -1 in (a) and (c) and by F in (d).

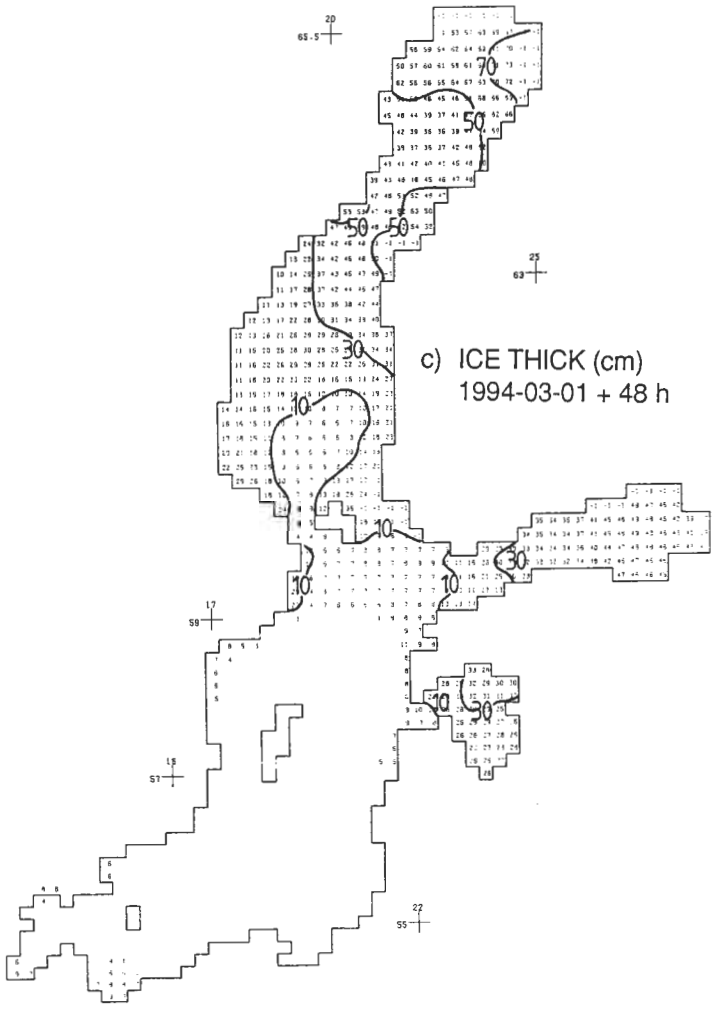

Figure 7 c.

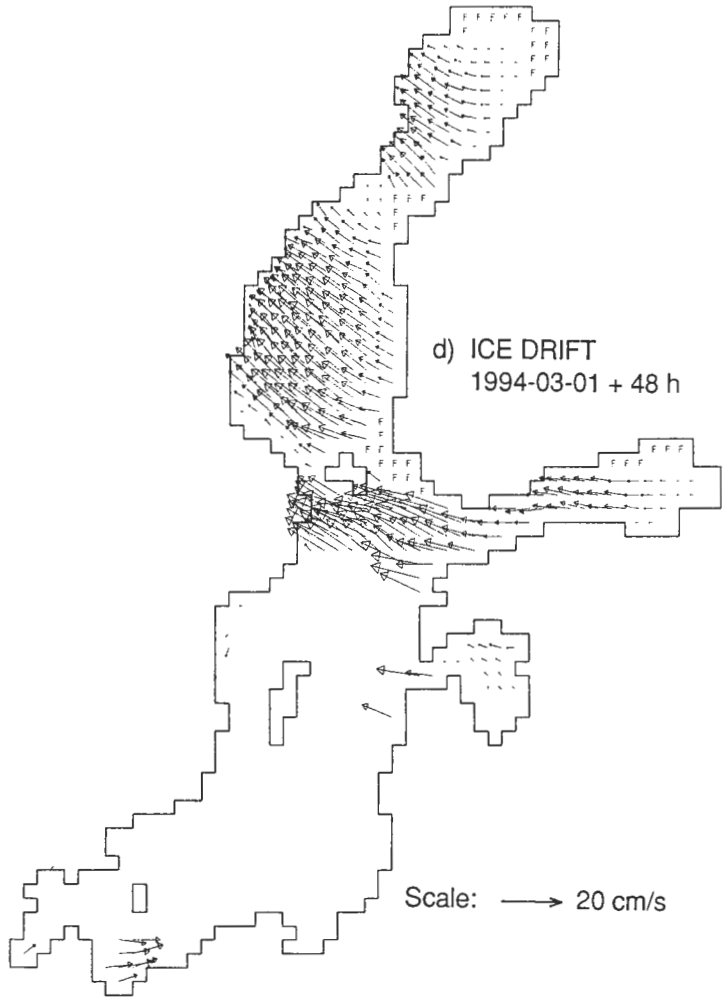

Figure 7 d.

4.3 Ice break-up and decay

The total ice mass in the Baltic Sea is strongly related both to thermodynamic and dynamic processes. This is illustrated by examining, calculated and observed ice from the middle of April (Figures 8 and 9). At that time we have passed the time for the maximum ice extent, ridging has increased the ice thickness and reduced the ice concentrations considerably. The calculations show most satisfactory results and, for example, that the calculated ice thicknesses vary between 60 and 100 cm at the north-west coast of the Bothnian Bay in good accordance with the observations.

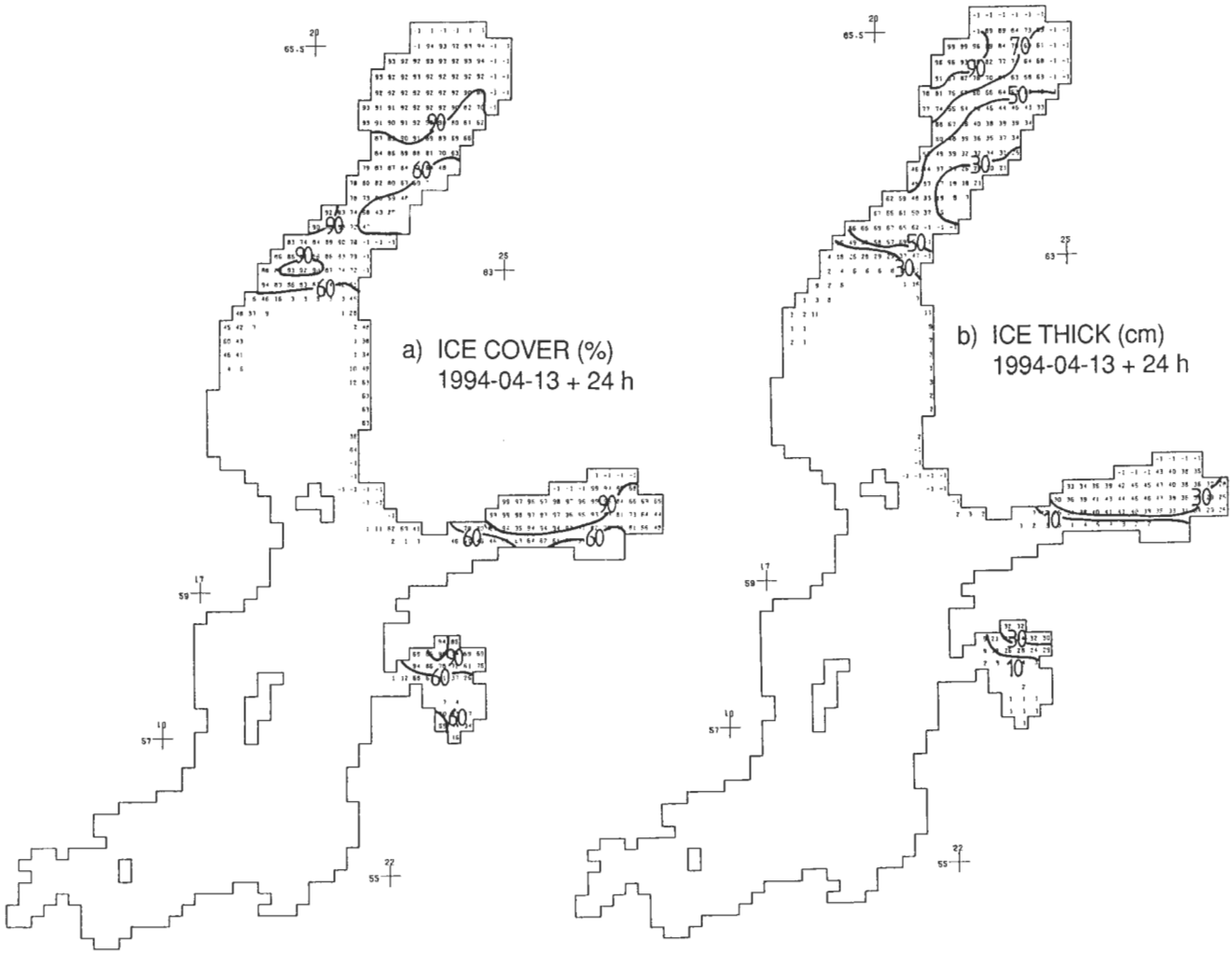

Figure 8.
Calculated ice concentrations (a) and ice thicknesses (b) on April 14, 1994.
Fast ice is denoted by -1.

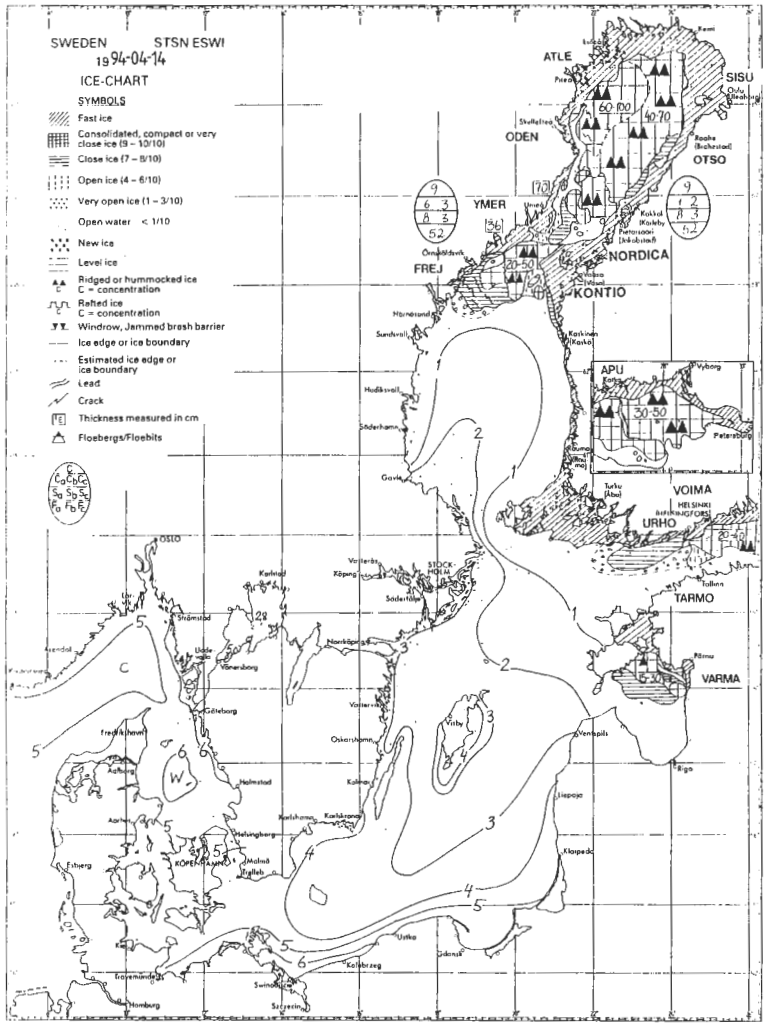

Figure 9.
Observed ice conditions on April 14, 1994.

4.4 Mean properties and seasonal variations

The model simulation of the whole ice season of 1993/94 was analysed by comparing observed and calculated horizontal mean properties. The Baltic Sea was divided into a number of verification areas (Figure 1), for which horizontal ice concentrations and thicknesses were digitalized on the basis of daily ice charts. The corresponding means were calculated in the model and the results from some of the subareas are illustrated below. The seasonal variations in the Bothnian Bay are illustrated in Figure 10. To interpret the comparison we need to recall that the thermodynamic calculations were performed in three

regions in the Bothnian Bay (Figure 2). Mean properties from all the three regions are given in the figure, and one should notice that when a region was ice-covered, it represented an ice-coverage of 100 % in that region. The water cooling, ice formation, ice growth and decay were well simulated in the Bothnian Bay. The break-up in the end of December, as was discussed in Section 4.1, can be noticed by the drastic change in ice concentration for region 3. Also the corresponding increase in surface temperatures due to mixing with deeper and warmer water can be noticed. The ice thicknesses are underestimated in the calculations. This is due to the fact that fast ice growth is neglected in the model but included in the digitalized values (see Section 4.3). The calculated ice thicknesses thus represent the drift ice, but the digitalized values also included landfast ice thickness.

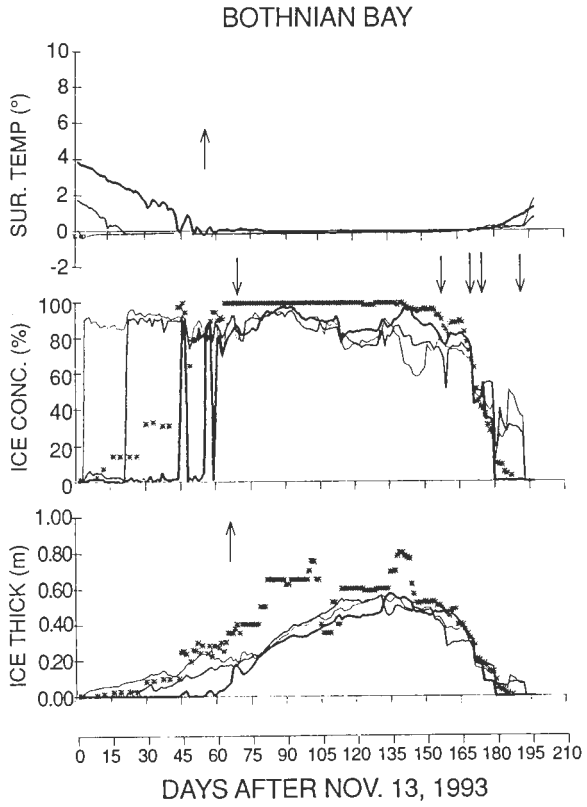

Figure 10.
Observed (stars) and calculated mean properties for the Bothnian Bay. The thin line represents region 1, the thicker region 2 and the thickest region 3 (see Figure 2). The arrows indicate when manual corrections of the initial fields were done.

The manual corrections of the initial fields are indicated by arrows in the figure. In the Bothnian Bay we only corrected water temperature and ice thickness once, however, ice concentration was corrected five times during the winter season. The corresponding results for some other regions are illustrated in Figures 11 - 14. In general, the mean properties were in good agreement with the observations on the ice charts. The model thus predicted initial ice formation and growth, interrupted freezing, melting and decay satisfactorily.

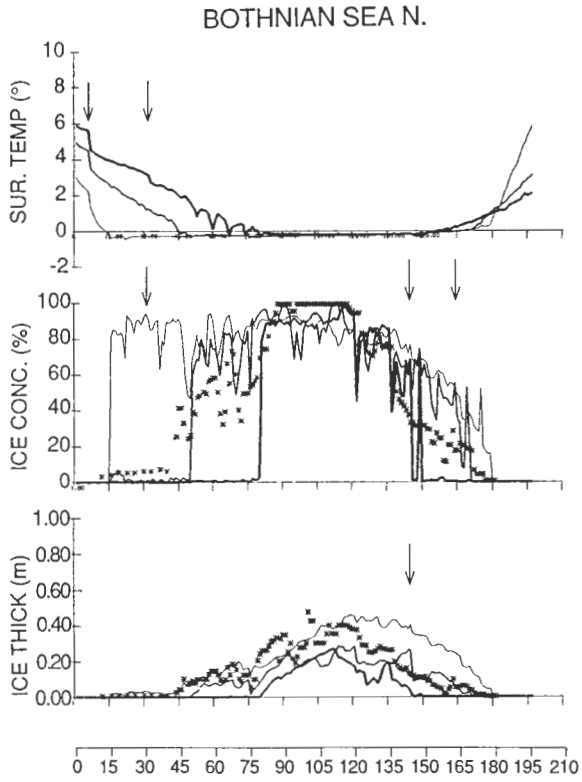

Figure 11.
Obseerved (stars) and calculated mean properties for the northern Bothnian Sea. The thin line represents region 4, thicker region 5 and the thickest region 6 (see Figure 2). The arrows indicate when manual corrections of the initial fields were done.

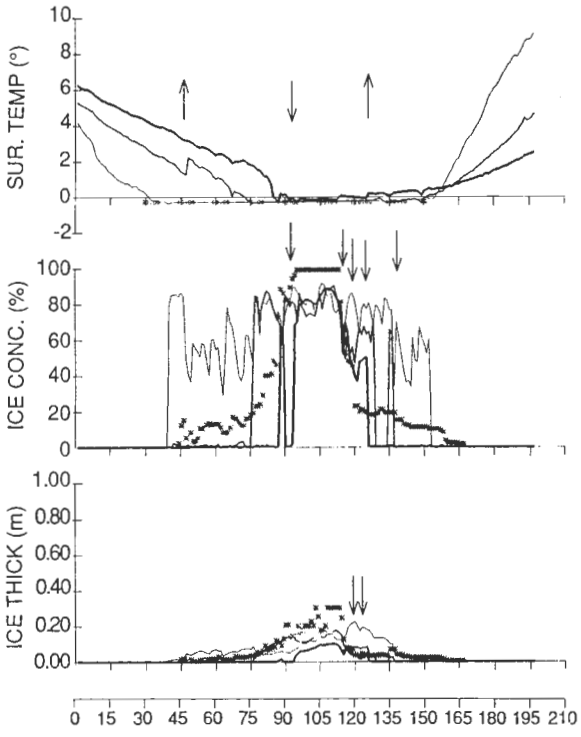

Figure 12.
Observed (stars) and calculated mean properties for the southern Bothnian Sea. The thin line represents region 7, the thicker region 8 and the thickest region 9 (see Figure 2). The arrows indicate when manual corrections of the initial fields were done.

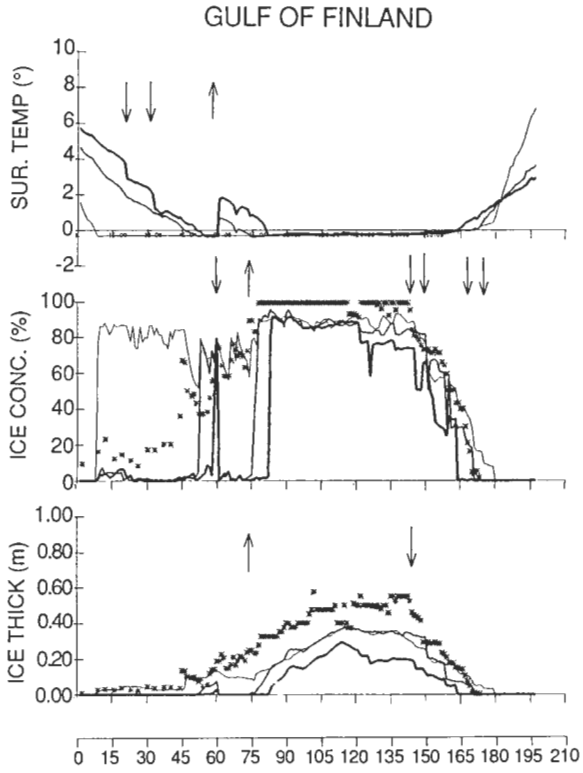

Figure 13.
Observed (stars) and calculated mean properties for the Gulf of Finland. The thin line represents region C, the thicker region D and the thickest region E (see Figure 2). The arrows indicate when manual corrections of the initial fields were done.

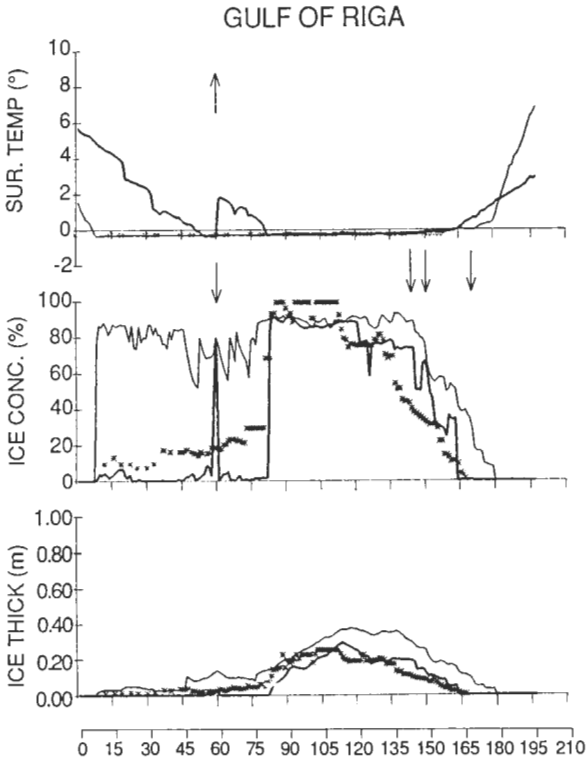

Figure 14.
Observed (stars) and calculated mean properties for the Gulf of Riga. The thin line represents region C, and the thicker region E (see Figure 2). The arrows indicate when manual corrections ot fhe initial fields were done.

5. METEOROLOGICAL COUPLING

The influence of the ice extent on weather forecasts in the Baltic Sea has recently been investigated by Andersson and Gustafsson (1994). They examined the formation of intense convective snow bands over the Baltic Sea by using HIRLAM and showed the importance of the shape of the coast from which the air departs and the coast at which it arrives. As the Baltic Sea costal geometry can change significantly due to sea ice, the change in the ice/water configuration during wintertime or, better, the sea ice concentration needs to be considered in accurate meteorological models.

During the winter of 1993/94, the HIRLAM system was not coupled to the BOBA-P19 model, instead a crude climate data base for sea surface temperatures and ice in the Baltic Sea was applied in the HIRLAM calculations. The accuracy of the HIRLAM forecast is discussed in Appendix B, where three synoptic stations representing the Baltic Sea were compared with the HIRLAM and ECMWF forecasts. In the verification study, there was no clear trend for the HIRLAM forecasts to be superior to the ECMWF forecasts. A higher resolution in HIRLAM in combination with an improved radiation scheme and a better treatment of sea surface temperatures and ice are therefore needed to improve the HIRLAM forecasts for the Baltic Sea.

The effects of coupling ice to HIRLAM were studied by making parallel runs with a new HIRLAM version. The new version was daily updated with ice concentration fields from the BOBA-P19 model and twice a week with observed sea surface temperatures. Below results from one simulation from 16 February, 1994, will be presented. In Figure 15, the HIRLAM concentration of ice in lakes and in the Baltic Sea are given. From the figure we can notice that the climate data base underestimates the ice concentrations in the Baltic Sea.

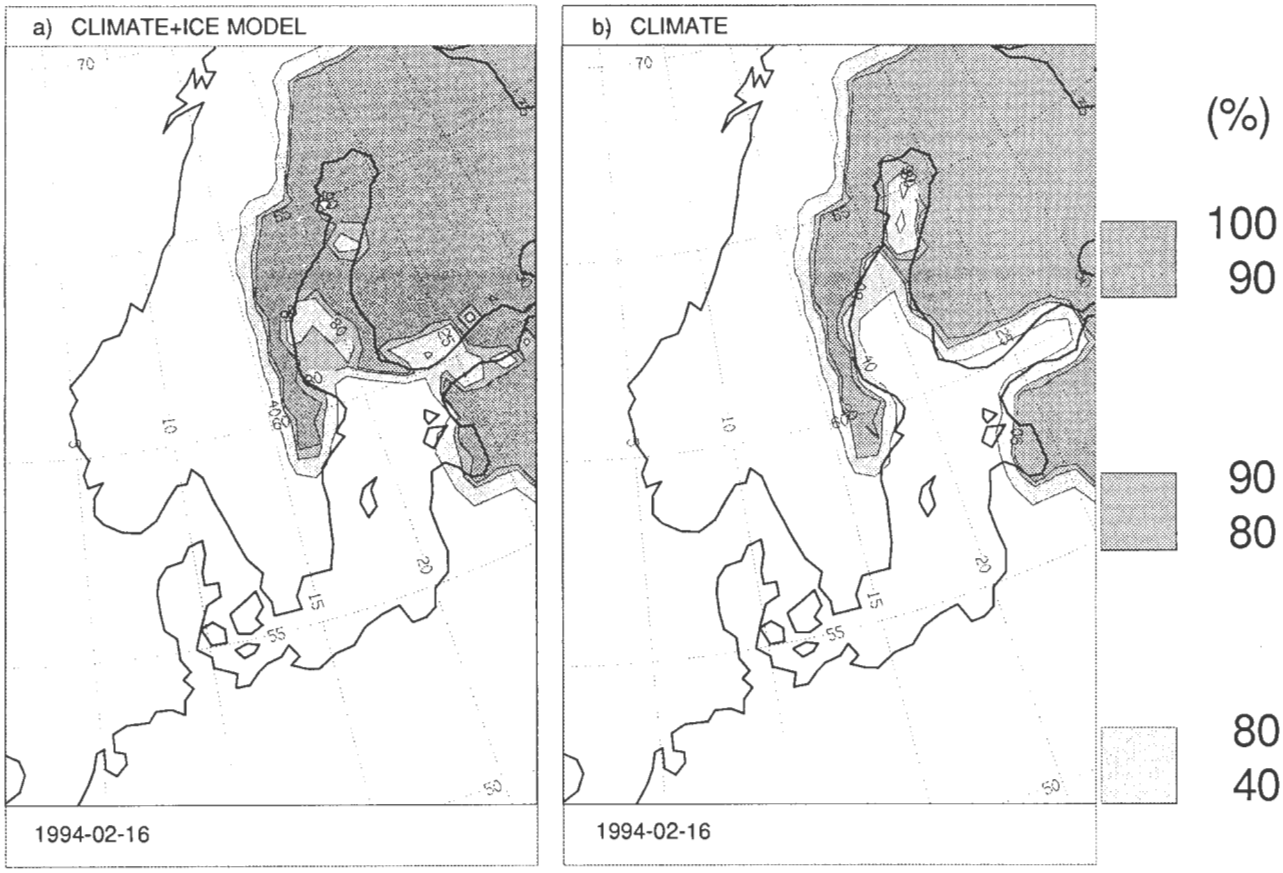

Figure 15.
Precentage of ice covered lakes and seas used by HIRLAM on February 28, 1994. In (a) climate data and ice concentrations from the ice model are illustrated compared to (b) where only climate data are given.

The corresponding forecasts of air temperature and winds are given in Figures 16 and 17. By comparing the two simulations we can notice that, particularly in the Bothnian Sea and the Gulf of Finland, the new HIRLAM version simulated colder temperatures and lower wind speeds. The HIRLAM system is thus sensitive to the sea surface temperature and the ice field in the Baltic Sea. Since April 1994, observed sea surface temperatures and calculated ice concentrations were therefore used in the operational HIRLAM version.

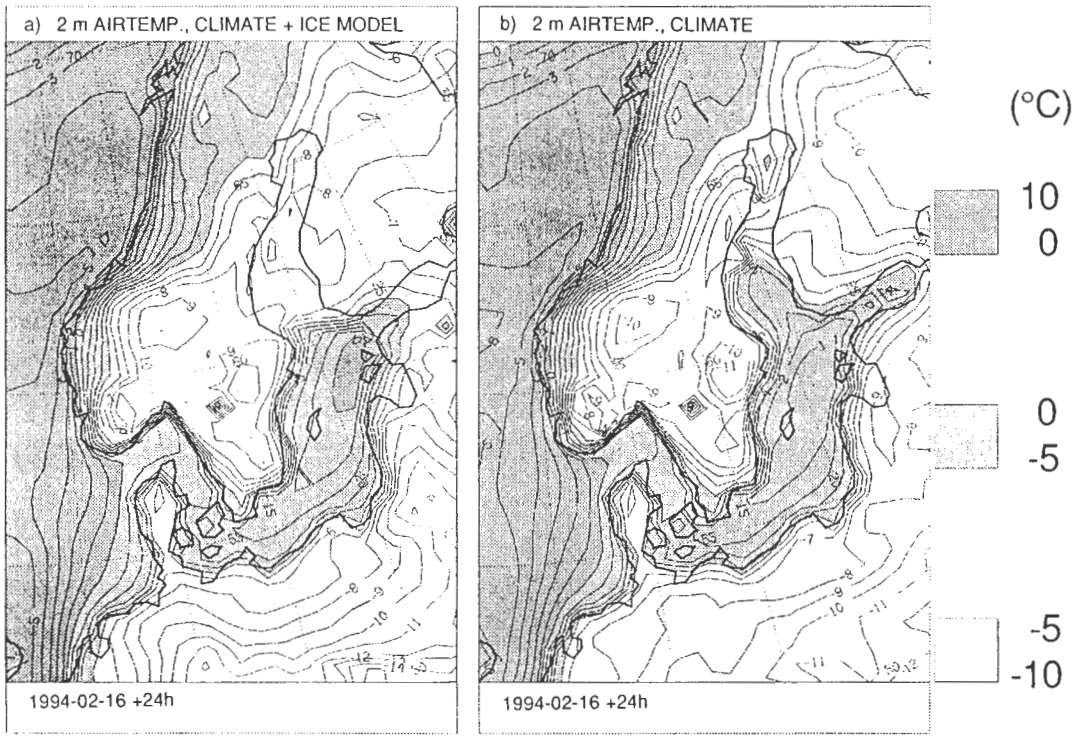

Figure 16.
A 24 hours´ HIRLAM forecast of air temperatures at 2 m height, based upon percentage of lakes and seas according to (a) climate data and ice model and (b) climate data only.

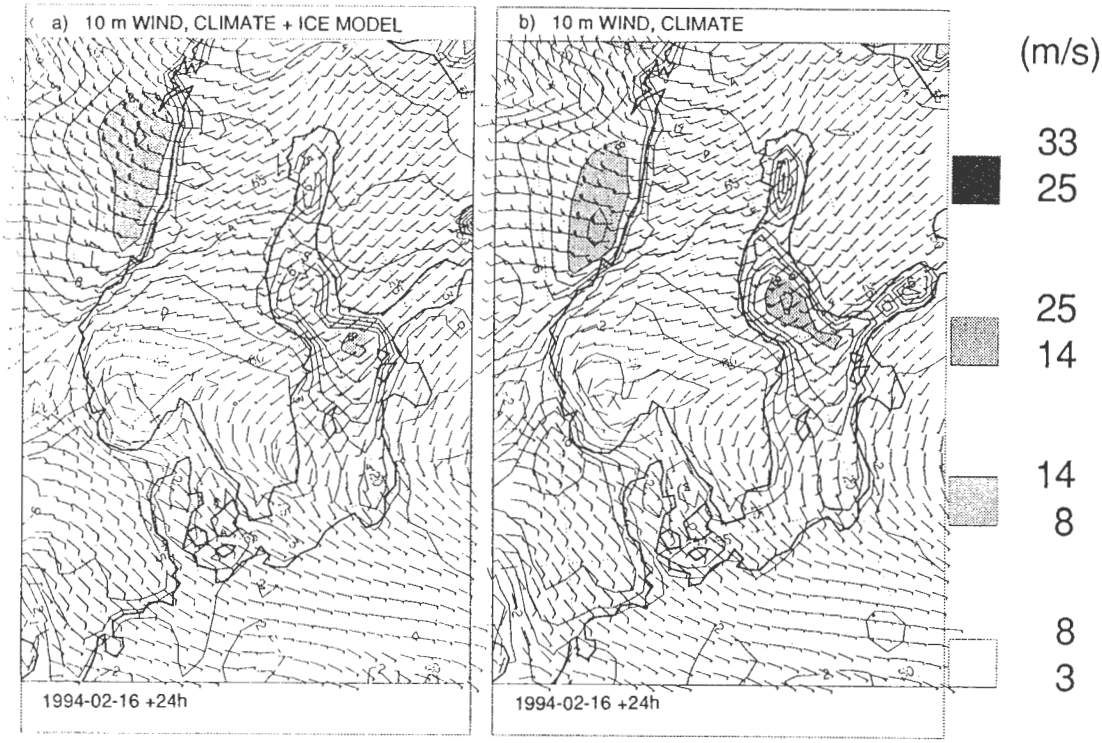

Figure 17.
A 24 hours HIRLAM wind forecast at 10 m height, based upon percentage of lakes and seas according to (a) climate data and ice model and (b) climate data only.

6. SUMMARY AND CONCLUSIONS

The winter navigation in the Baltic Sea is strongly influenced by sea ice. It is therefore important to develop accurate forecast models for sea ice. In the present report we have presented a coupled ice-ocean model for the Baltic Sea. The dynamical part of the model is based on a Hibler type ice model, which has been further developed in Finland, and a storm surge model developed in China. The thermodynamic part of the model is based upon boundary layer models developed in Sweden.

For the thermodynamic part the equations were solved in the vertical space and time, calculating water cooling, ice formation, ice growth and decay and water warming in 19 different regions of the Baltic Sea. During the winter of 1992/93 the dynamical part of the model was used in operational mode (Omstedt et al., 1994), and during the winter of 1993/94 the full model including thermodynamics was run in operational mode.

The meteorological forcing fields have been taken from the HIRLAM system. During the winter of 1993/1994 some tests with a closer coupling between the ice-ocean model and HIRLAM have been run. The results from these tests have shown the importance of using accurate ice data in the HIRLAM forecast. The new version of HIRLAM will therefore use the calculated ice concentration fields from the ice-ocean model as daily input. This is a great step forward in the winter navigation research and will probably give more accurate forecasts in the future.

For the first time a coupled ice-ocean model simulating both dynamic and thermodynamic processes has been used in operational service for the Baltic Sea. The model forecasts water cooling, ice formation, ice growth and decay, ice drift, ice ridging, sea level variations and water warming in a satisfactory way. Also for the first time we have been able to couple the ice-ocean model closer to the meteorological model. The model system forms a good base for forecasts and research. Updating the meteorological model with calculated ice concentration is the first step, but further work and experiments will be made on the exchange of data between the ice and the HIRLAM systems and improvements of the atmosphere boundary layer parametrization above open and ice-covered sea areas. In future automatic methods for creating initial data to the model also need to be developed.

ACKNOWLEDGEMENTS

This work is a part of the Swedish-Finnish Winter Navigation Research Programme and has been financed by the Swedish National Maritime Administration and by SMHI. We would like to thank Jan Stenberg for his interest and support during the work. We would also like to thank Nils Gustavsson, Lars Häggmark and Lars Meuller for assistance with the HIRLAM model, George Ericsson for verification of HIRLAM and Stig Nilsson for digitalizing the ice charts. Vera Kuylenstierna and Gun Sigurdsson corrected and typed the manuscript, which is gratefully acknowledged.

REFERENCES

Andersson, T., and Gustafsson, N. (1994)
Coast of departure and coast of arrival: Two important concepts for the formation and structure of convective snow bands over seas and lakes.
Monthly Weather Review, 122, No. 6, 1036 - 1049.

Bodin, S. (1979)
A predictive numerical model of the atmospheric boundary layer based on the turbulent energy equation.
Report Meteorology and Climatology No. 13, SMHI, S-601 76 Norrköping, Sweden, 139 pp.

Friehe, C.A., and Schmitt, K.F. (1976)
Parameterization of air-sea interface fluxes of sensible heat and moisture by the bulk aerodynamic formulae.
J. Phys. Oceanogr. 6, 801 - 809.

Gustafsson, N., Bringfelt B. and Järvenuja S. (1994) :
Tests of a new radiation scheme and new surface fields. In HIRLAM Newsletter, No 15. Available from SMHI, S-601 76 Norrköping, Sweden.

Hibler III, W.D. (1979)
A dynamic thermodynamic sea ice model.
J. Phys. Oceanogr., 9(4), 815 - 846.

Leppäranta, M. (1981)
An ice drift model for the Baltic Sea.
Tellus, 33, 583 - 596.

Leppäranta, M., and Omstedt, A. (1990)
Dynamic coupling of sea ice and water for an ice field with free boundaries.
Tellus, 42A, 482 - 495.

Leppäranta, M., and Zhang, Zh.-H. (1992)
Use of ERS-1 SAR data in numerical sea ice modeling.
Proc. Central Symp. ISY Conf. (ESA SP-341), 123 - 128.

Maykut, G.A. (1986)
The surface heat and mass balance.
In: The Geophysics of Sea Ice. (Ed. N. Untersteiner.) The NATO ASI Series, B 146. New York, USA. Plenum, 395 - 463.

McPhee, M., Maykut, G.A., and Morrison, J.H. (1987)
Dynamics and thermodynamics of the ice/upper ocean system in the marginal ice zone of the Greenland Sea.
J. Geophys. Res., 92, 7017 - 7031.

Mellor, G.L., McPhee, M.G., and Steele, M. (1986)
Ice-sea water turbulent boundary layer interaction with melting and freezing.
J. Phys. Oceanogr., 16, 1829 - 1846.

Omstedt, A. (1990 a)
A coupled one-dimensional sea ice-ocean model applied to a semi-enclosed basin.
Tellus, 42A, 568 - 582.

Omstedt, A. (1990 b)
Modelling the Baltic Sea as thirteen sub-basins with vertical resolution.
Tellus, 42A, 286 - 301.

Omstedt, A. (1990 c)
Real-time modelling and forecasting of temperatures in the Baltic Sea.
SMHI Reports, RO 12.

Omstedt, A., Nyberg, L., and Leppäranta, M. (1994)
A coupled ice-ocean model supporting winter navigation in the Baltic Sea. Part 1: Ice dynamics and water levels.
SMHI Reports, RO 17, 17 pp.

Omstedt, A., Sahlberg, J., and Svensson, U. (1983)
Measured and numerical simulated autumn cooling in the Bay of Bothnia.
Tellus, 35A, 231 - 240.

Sahlberg, J. (1988)
Modelling the thermal regime of a lake during winter season.
Cold Region Science and Technology, 15, 151 - 159.

Seinä, A., and Palosuo, E. (1993)
The classification of the maximum annual extent of ice cover in the Baltic Sea 1720 - 1992. (In Finnish.)
Meri, No. 20, 5 - 20.

Svensson, U. (1986)
PROBE - An instruction manual.
Report Oceanography No. 10, SMHI, S-601 76 Norrköping, Sweden, 90 pp.

Svensson, U. (1979)
The structure of the turbulent Ekman layer.
Tellus, 31, 340 - 350.

Svensson, U., and Omstedt, A. (1990)
A mathematical model of the ocean boundary layer under drifting melting ice.
J. Phys. Oceanogr., 20, 161 - 171.

Yaglom, A.M., and Kader, B.A. (1974)
Heat and mass transfer between a rough wall and turbulent fluid flow at high Reynolds and Peclet numbers.
J. Fluid Mech., 62, 601 - 623.

Zhang, Zh.-H., and Leppäranta, M. (1992)
Modeling the influence of sea ice on water in the Gulf of Bothnia.
Internal Report 4, Finnish Institute of Marine Research.

Zhang, Zh.-H., and Wu, H.-D. (1990)
Numerical simulation for storm surges in the China Sea. (In Chinese.)
Marine Forecasts 7(2), 10 - 19.

APPENDIX A. Parametrization of heat fluxes

The parametrization of the different energy fluxes in Equation (22) as well as the heat source term Γ_s in Equation (5) are outlined below. Together they form a heat flux package (PROBEFLX) which has been applied in several lake and ocean simulations at the SMHI during the last ten years.

The sensible and latent heat fluxes are driven by the temperature and the moisture differences between water/air, respectively. The parametrization follows Friehe and Schmitt (1976), where different transfer coefficients are introduced depending on stratification conditions. The fluxes read:

$$F_h = \rho_a c_{pa}(C_1 + C_h W_a(T_s - T_a)) \tag{A1}$$

$$F_e = L_e C_e W_a(q_w - q_a) \tag{A2}$$

where ρ_a (= 1.3 kg m^{-3}) is the air density, C_{pa} (= 1016 J kg^{-1} K^{-1}) the specific heat of air, C_h and C_e are the sensible heat and the latent heat transfer coefficients, respectively, C_1 is a constant, T_s the surface water temperature W_a the wind velocity at 10 m, L_e (= 2.5 • 10^6 J kg^{-1}) the latent heat of evaporation, q_w and q_a are the water vapour density close to the water surface and in the atmosphere, respectively. The numbers put in brackets are values used in the present application. Measurements of q_w and q_a are not directly available, instead they are transformed to functions of temperatures and relative humidity. The bulk heat transfer coefficients read:

$$(C_1, C_h) = \begin{cases} 0.0026,\ 0.86 \cdot 10^{-3} & \text{when } W_a(T_s - T_a) < 0, \\ 0.002,\ 0.97 \cdot 10^{-3} & \text{when } 0 \le W_a(T_s - T_a) \le 25, \\ 0.0,\ 1.46 \cdot 10^{-3} & \text{when } W_a(T_s - T_a) > 25, \end{cases}$$

and $C_e = 1.36\ C_h$ for all stabilities.

The net long-wave radiation is due to atmospherical and water surface radiation. The formulation reads:

$$F_{lu} - F_{ld} = \varepsilon_w \sigma_s \left[T_w^4 - T_a^4\left(a_1 + a_2\sqrt{e_a}\right)\left(1 + a_3 N_a^2\right)\right] \tag{A3}$$

where ϵ_w (= 0.97) is the emissivity of the water surface, e_a the water vapour pressure in the atmosphere, σ_s (= 5.67 · 10^{-8} W m^{-2} K^{-4}) the Stefan Bolzman's constant, N_a the cloud coverage, and a_1, a_2 and a_3 are constants equal to 0.68, 0.0036 and 0.18, respectively.

Short-wave radiation penetrates down into the water column either through the open sea surface or through the ice cover, and increases the heat content due to internal absorption. The short-wave energy flux penetrating the open water surface reads:

$$F_s^w = F_s(1 - \alpha_w) \tag{A4}$$

where F_s is the insolation towards the surface and α_w is the surface water albedo calculated from the Fresnels formula.

The insolation towards the ground can be calculated from:

$$F_s = T_u S_0 \cos\Theta (T_r - A_w)(1 - N_a F_a) \tag{A5}$$

where T_u is the atmospherical turbidity which is put equal to 0.95, S_0 (= $1.36 \cdot 10^3$ J m^{-2} s^{-1}) the solar constant, Θ the zenith angle, T_r and A_w are transmission and absorption functions, and F_a is a cloud function. The short- and long-wave formulations follow those by Bodin (1979), but with only the total cloud amount considered in the present application. The expressions then read:

$F_a = 0.55 + 0.01 \cos\Theta^{-1}$,
$T_r = 1.041 - 0.16 \cos\Theta^{-0.5}$,
$A_w = 0.077\, m^{0.3} \cos\Theta^{-0.3}$,

where m is the optical path length, which is calculated as a function of season.

The modelling of the short-wave radiation, which penetrates snow and ice, follows that by Sahlberg (1988). The equation reads:

$$F_s^{ib} = F_s(1 - \alpha_s) i_{os} e^{-\overline{K}_s (h_s - 0.1) - \overline{K}_i h_i} \tag{A6}$$

where α_s (= 0.75) is the snow albedo, i_{os} (= 0.1) is a penetration factor, h_s the snow thickness, h_i the ice thickness, $\overline{K}_s$ (= 15 m^{-1}) and $\overline{K}_i$ (= 1.5 m^{-1}) the bulk extinction coefficients for snow and ice, respectively. Basic assumptions in Eq. (A6) are that slush is not present and that the snow depth is equal to or larger than 0.1 m. The corresponding expression for the short-wave radiation at the top of the ice surface reads:

$$F_s^{it} = F_s(1 - \alpha_s) \tag{A7}$$

The solar radiation penetrates down into the water column and increases the heat content due to internal absorption. An exponential decay law is assumed, and the heat source term

Γ_s due to solar radiation to the open water surface and through the ice reads:

$$\Gamma_s = -\left[F_s^w(1 - A_i) + F_s^{ib}A_i\right](1 - \eta)\beta e^{-\beta(D - z)} \tag{A8}$$

where η is a measurement of the infrared content of the solar radiation, D the total water depth, z the vertical space coordinate positive upwards, and β an absorption coefficient. The constants η and β are put equal to 0.4 and 0.3, respectively.

The heat flux between water and ice is calculated from one dimensional ocean model, and the formulation reads:

$$F_w = \rho C_p\left(\frac{\nu}{Pr_L} + \frac{\nu_T}{Pr_T}\right)\frac{\partial T}{\partial z} \tag{A9}$$

where ρ is the density of water, C_p the specific heat or water, T the water temperature, ν and ν_T are the kinematic laminar and turbulent viscosity and Pr_L and Pr_T the laminar and turbulent Prandtl numbers.

The heat flux associated with ice advection, F_i, assuming that all ice advected into the sea area is melted, reads:

$$F_i = \frac{Q_{ice}}{\Delta A} L_i \rho_i \tag{A10}$$

where Q_{ice} is the advected flow of ice into the next grid cell, L_i the latent heat of ice, ρ_i the ice density and ΔA the area of the grid cell.

APPENDIX B. Verification study of the HIRLAM system over the Baltic Sea

The energy flux calculations require information about air temperature, wind, relative humidity and total amount of clouds. For the oceanic storm surge model, atmospheric pressure is also needed. During the winter of 1993/94, the HIRLAM system with a resolution of 55 km was used for the generation of the meteorological forcing fields. In the present appendix, some verification results of the HIRLAM system for the winter period 1 November, 1993, to 30 April, 1994, are given. During this period, the HIRLAM system applied a crude climate data base for ice and sea surface temperatures in the Baltic Sea. Some tests with coupling of the sea ice model to HIRLAM were performed (Section 5), but in the verification results below, these effects were not yet included. In the statistics mean, root mean and square errors were calculated. The definition of the statistics are as follows:

Mean error (ME)= $\frac{1}{N} \sum_{1}^{N} (f_n - o_n)$

Root mean square error (RMSE) =

$$\sqrt{\frac{1}{N} \sum_{1}^{N} (f_n - o_n)^2}$$

where f_n and o_n are the forecast and observation values, respectively, and N is the number of values. For the total cloudiness, the forecast and observation values were divided into 3 categories defined as: cloudiness less than 3/8, equal or larger than 3/8 and smaller than 7/8, and above or equal to 7/8.

In the statistical study, both the 0 and the 12 UTC HIRLAM forecasts as well as the 12 UTC ECMWF forecast have been analysed. Below we only present results from three stations representing the northern, the central and the southern Baltic Sea. The stations are Holmögadd, Gotska Sandön and Rönne; see Figures B1 - B6.

The 24 hours' forecast of air pressure which was used for the updating of the oceanic storm surge model, shows an RMSE of about 2 h Pa corresponding to a water level error of 2 cm. The ME was less and slightly positive, indicating a higher pressure in the forecast compared to the observations.

In the temperature forecasts, we can notice that Holmögadd had the largest errors corresponding to an RMSE of about 3 (°C). The temperature ME from Holmögadd showed that the HIRLAM forecasts were colder than observed, but for Gotska Sandön and Rönne the mean errors varied around 0 (°C). This illustrates that the HIRLAM grid cell close to Holmögadd was much influenced by land. A better resolution in HIRLAM should be expected to give better results.

For the wind forecasts, the RMSE for the 48 hours' forecasts were better than 4 m/s. The ME showed that the predicted winds were underestimated for Holmögadd but the error varied around 0 for the other two stations. Again this illustrates that Holmögadd was more influenced by land than the other two stations. Thus we can notice that both temperatures and winds were to low at Holmögadd. For the ice production, however, these errors

balance each other, as a colder temperature gives higher heat fluxes but a lower wind reduces the fluxes. The forecasts of total cloudiness show that HIRLAM underestimates the cloudiness.

A recent verification study of HIRLAM with modified physical parameterization schemes (Gustafsson et al 1994) has indicated that HIRLAM low level temperatures are too cold during the late winter and early spring periods, due to weaknesses in the operational radiation scheme. This is clearly seen in the temperature forecasts for Holmögadd. In addition, it has also been possible to prove that these too cold low level temperatures are causing an inflow of mass over the horizontal boundaries of the integration area (also seen in the pressure forecasts for Holmögadd). Furthermore, wind velocity forecasts for Baltic Sea coastal areas in general underestimate the true wind velocities and this has been found to be related to unrealistically large values of surface roughness lengths due to vegetation. A new version of HIRLAM with an improved radiation scheme and with new surface fields, like roughness length, will be introduced during the autumn 1994.

There was no clear trend for the HIRLAM forecasts to be superior to the ECMWF forecasts. For example, at Holmögadd, the HIRLAM temperatures were better, but the pressure fields and winds from ECMWF were better than those from the HIRLAM forecasts. However, verification studies over land during the winter period show in general that the HIRLAM forecasts were better compared to the ECMWF forecasts. A higher resolution in HIRLAM in combination with an improved radiation scheme and a better treatment of ice and sea surface temperatures are therefore needed before HIRLAM forecasts become better than ECMWF forecasts over the Baltic Sea.

HOLMÖGADD

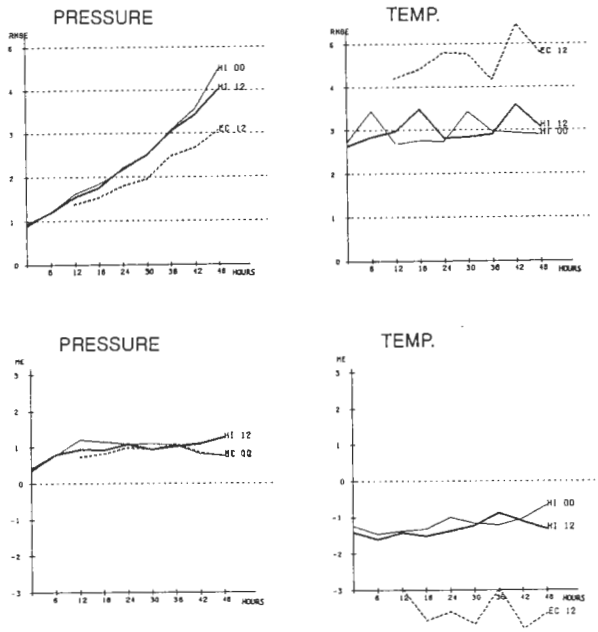

Figure B 1.
Mean error (ME) and root mean square error (RMSE) based upon data from Holmögadd for the period 1 November, 1993 to 30 April 1994 compared to the HIRLAM (HI) 00 and 12 UTC forecast and the ECMWF (EC) 12 UTC forecast.

HOLMÖGADD

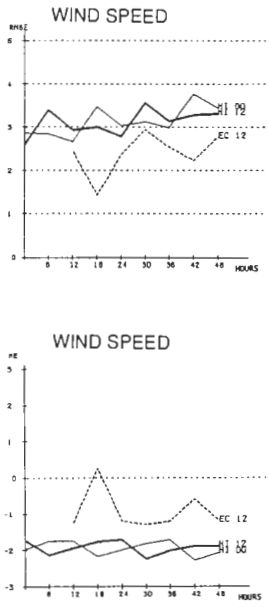

CLOUD

KATEG.		1	2	3
		OBSERVATION		
KATEG. 1	FORECAST	24	22	7
KATEG. 2		5	12	26
KATEG. 3		3	9	73

Figure B 2.
Same legend as for Fig. B 1. The cloud categories are defined in the text.

GOTSKA SANDÖN

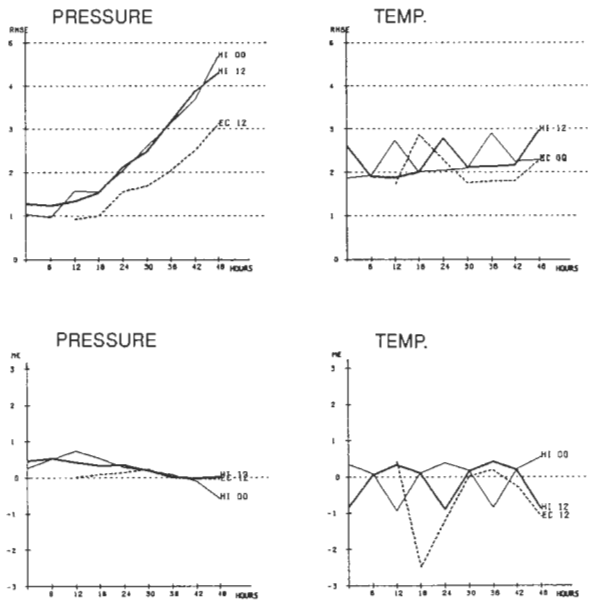

Figure B 3.
Same legend as for Fig. B 1, but for Gotska Sandön.

GOTSKA SANDÖN

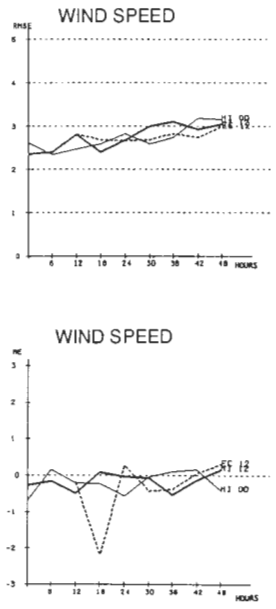

CLOUD

KATEG.		1	2	3
		OBSERVATION		
KATEG.	1	31	10	20
KATEG.	2	13	8	19
KATEG.	3	7	10	62

FORECAST

Figure B 4.
Same legend as for Fig. B 1, but for Gotska Sandön. The cloud categories are defined in the text.

RÖNNE

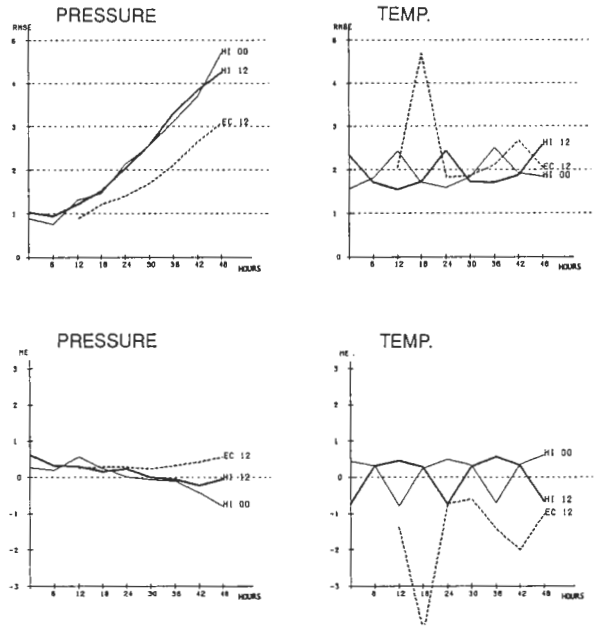

Figure B 5.
Same legend as for Fig. B 1, but for Rönne.

RÖNNE

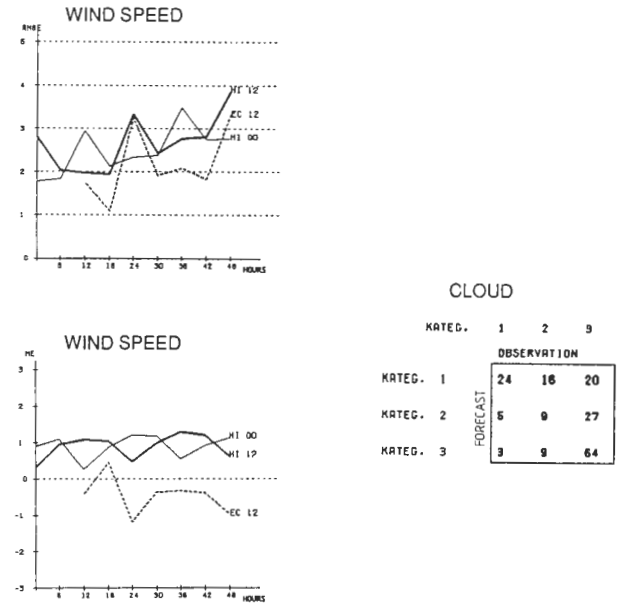

Figure B 6.
Same legend as for Fig. B 1, but for Rönne. The cloud categories are defined in the text.

SMHI rapporter OCEANOGRAFI (RO)

Nr Titel

1 Lars Gidhagen, Lennart Funkquist and Ray Murthy.
Calculations of horizontal exchange coefficients using Eulerian time series current meter data from the Baltic Sea.
Norrköping 1986.

2 Thomas Thompson.
Ymer-80, satellites, arctic sea ice and weather.
Norrköping 1986.

3 Stig Carlberg et al.
Program för miljökvalitetsövervakning - PMK.
Norrköping 1986.

4 Jan-Erik Lundqvist och Anders Omstedt.
Isförhållandena i Sveriges södra och västra farvatten.
Norrköping 1987.

5 Stig Carlberg, Sven Engström, Stig Fonselius, Håkan Palmén, Eva-Gun Thelén, Lotta Fyrberg och Bengt Yhlen.
Program för miljökvalitetsövervakning - PMK. Utsjöprogram under 1986.
Göteborg 1987.

6 Jorge C. Valderama.
Results of a five year survey of the distribution of UREA in the Baltic sea.
Göteborg 1987.

7 Stig Carlberg, Sven Engström, Stig Fonselius, Håkan Palmén, Eva-Gun Thelén, Lotta Fyrberg, Bengt Yhlen och Danuta Zagradkin.
Program för miljökvalitetsövervakning - PMK. Utsjöprogram under 1987.
Göteborg 1988.

8 Bertil Håkansson.
Ice reconnaissance and forecasts in Storfjorden, Svalbard.
Norrköping 1988.

9 Stig Carlberg, Sven Engström, Stig Fonselius, Håkan Palmén, Eva-Gun Thelén, Lotta Fyrberg, Bengt Yhlen, Danuta Zagradkin, Bo Juhlin och Jan Szaron.
Program för miljökvalitetsövervakning - PMK. Utsjöprogram under 1988.
Göteborg 1989.

10 L. Fransson, B. Håkansson, A. Omstedt och L. Stehn.
Sea ice properties studied from the icebreaker Tor during BEPERS-88.
Norrköping 1989.

Nr Titel

11 Stig Carlberg, Sven Engström, Stig Fonselius, Håkan Palmén, Lotta Fyrberg, Bengt Yhlen, Bo Juhlin och Jan Szaron.
Program för miljökvalitetsövervakning - PMK. Utsjöprogram under 1989.
Göteborg 1990.

12 Anders Omstedt.
Real-time modelling and forecasting of temperatures in the Baltic Sea.
Norrköping 1990.

13 Lars Andersson, Stig Carlberg, Elisabet Fogelqvist, Stig Fonselius, Håkan Palmén, Eva-Gun Thelén, Lotta Fyrberg, Bengt Yhlen och Danuta Zagradkin.
Program för miljökvalitetsövervakning - PMK. Utsjöprogram under 1990.
Göteborg 1991.

14 Lars Andersson, Stig Carlberg, Lars Edler, Elisabet Fogelqvist, Stig Fonselius, Lotta Fyrberg, Marie Larsson, Håkan Palmén, Björn Sjöberg, Danuta Zagradkin, och Bengt Yhlen.
Haven runt Sverige 1991. Rapport från SMHI, Oceanografiska Laboratoriet, inklusive PMK - utsjöprogrammet.
(The conditions of the seas around Sweden. Report from the activities in 1991, including PMK - The National Swedish Programme for Monitoring of Environmental Quality Open Sea Programme.)
Göteborg 1992.

15 Ray Murthy, Bertil Håkansson and Pekka Alenius (ed.).
The Gulf of Bothnia Year-1991 - Physical transport experiments.
Norrköping 1993.

16 Lars Andersson, Lars Edler and Björn Sjöberg
The conditions of the seas around Sweden. Report from activities in 1992.
Göteborg 1993.

17 Anders Omstedt, Leif Nyberg and Matti Leppäranta.
A coupled ice-ocean model supporting winter navigation in the Baltic Sea.
Part 1. Ice dynamics and water levels.
Norrköping 1994.

18 Lennart Funkquist.
An operational Baltic Sea circulation model. Part 1. Barotropic version.
Norrköping 1993.

19 Eleonor Marmefelt
Currents in the Gulf of Bothnia. During the Field Year of 1991.
Norrköping 1994.

20 Lars Andersson, Björn Sjöberg and Mikaell Krysell
The conditions of the seas around Sweden. Report from the activities in 1993.
Göteborg 1994.

21 Anders Omstedt and Leif Nyberg
A coupled ice-ocean model supporting winter navigation in the Baltic Sea.
Part 2. Thermodynamics and meteorological coupling.
Norrköping 1995.

SMHI
Swedish meteorological and hydrological institute
S-60176 Norrköping, Sweden. Tel. +4611158000. Telex 64400 smhi s.

ISSN 0283/1112